CAPABILITY OF LANDSAT-8/SPOT-6 IN QUANTIFYING CHLOROPHYLL-*a* IN INLAND LAKES

CHRISTIAN KWESI OWUSU

February, 2016

SUPERVISORS:
Dr. Ir. Mhd. Suhyb Salama
Prof. Dr. Ing. Wouter Verhoef

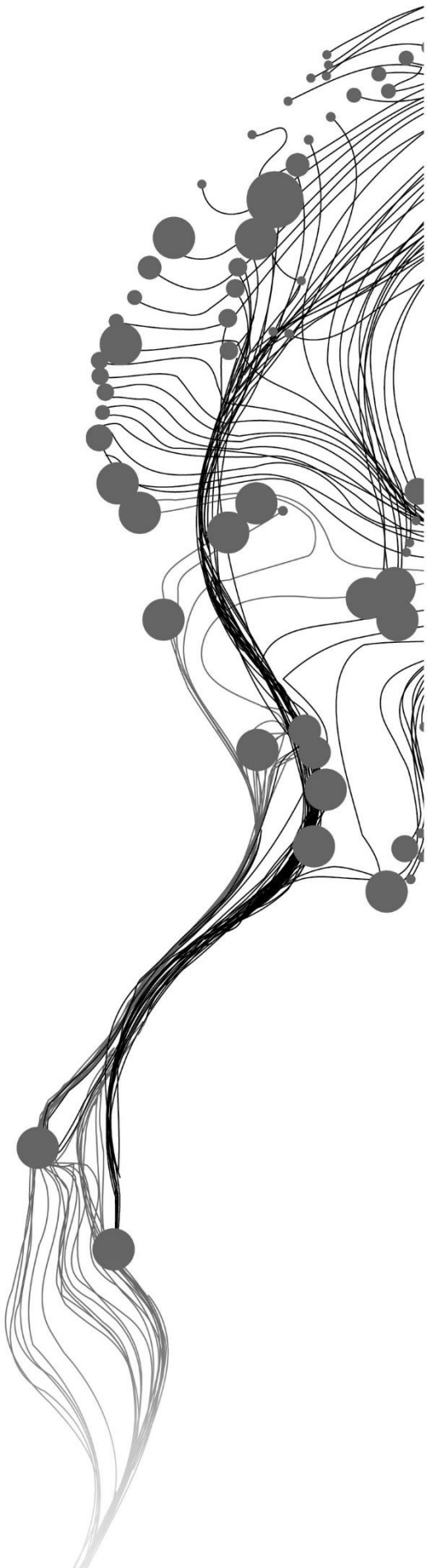

CAPABILITY OF LANDSAT-8/SPOT-6 IN QUANTIFYING CHLOROPHYLL-*a* IN INLAND LAKES

CHRISTIAN KWESI OWUSU

Enschede, The Netherlands, February, 2016

Thesis submitted to the Faculty of Geo-Information Science and Earth Observation of the University of Twente in partial fulfilment of the requirements for the degree of Master of Science in Geo-information Science and Earth Observation.
Specialization: Water Resources and Environmental Management

SUPERVISORS:
Dr. ir. Mhd. Suhyb Salama
Prof. Dr. Ing. Wouter. Verhoef

THESIS ASSESSMENT BOARD:
Dr. Ir. C.M.M. (Chris) Mannaert, (Chair)
Ing. L. (Leontien) van der Molen, (External Examiner, Advisor Water-systems Water board, Vechtstromen)

ABSTRACT

The use of satellite remote sensing in monitoring chlorophyll-a pigments in all marine and fresh open inland water has been a significant issue in the past decades for preserving and monitoring ecological issues related to aquatic systems.

Three small lakes in the Netherlands were used to study Chlorophyll-a (absorption coefficient of pigments/phytoplankton) estimation based on band ratio algorithms using concurrent in-situ on one hand, and Landsat-8 and SPOT6 data. This study identified, adapted and tested the performance of four (4) empirical models based on optimal bands using both satellite sensor data and field radiometric data for proper assessment of Chlorophyll-a. Each of the algorithms specifically requires an optimal band(s) and these bands differ among the algorithms. These algorithms includes Maximum Chlorophyll-*a* Index (MCI), the Three Band Model (TBS/3B), Normalized Differential Index Model (NDCI), and the Four Band Model (FBS). Ground sourced data including spectral reflectance data and absorption coefficient of chlorophyll-a pigments/phytoplankton were used for further analysis. The models were tuned and validated using the Geo-Cal/Val method.

In-situ variations of absorption coefficient of chlorophyll-a were compared with modelled/estimated absorption coefficient of chlorophyll-a pigments/phytoplankton using four different band ratio algorithms. Good correlation was found when models were applied on in-situ data than concurrent Landsat-8 and SPOT6 data. The FBS/4B algorithm performed well with in-situ data, with an R^2, of 0.83 respectively and a minimal percentage error of (rMAE) 12.35%. However, the MCI model performed better than the FBS/4B as well as the 3B and NDCI models when applied to both Landsat-8 and SPOT6 data.

Only few images processed through FLAASH and was used to depict the distribution and variation of Chl-a concentration (a_phy) over Lake Binnenschelde, Markiezaatsmeer and Hulsbeek retrieved via the application of the MCI band ratio-ing. It is also found that FLAASH is not suitable for atmospheric correction of SPOT6 images intended for this study.

Comparison of sensors showed that Landsat-8 performed better that SPOT6 in the derivation of absorption coefficient of chlorophyll-a pigments/phytoplankton. The MCI model maintained its consistency in working well with all the various data set and was found better than all other models, hence it was chosen as the best model. It had an R^2 of 0.69 when applied on in-situ data, and R^2 of 0.75 for Landsat-8 data as well 0.58 for SPOT6 data. The MCI percentage error was comparatively low for Landsat-8 (21.29%) and in-situ data (18.34%) showing only 3% increase in error but error doubled when MCI was applied on SPOT6 data. In all, most of the algorithms used in this study were sensitive to estimating absorption coefficients of Chl-a from both in-situ and Landsat-8 data.

Keywords: Chlorophyll-a, absorption of chlorophyll-a, Landsat-8, SPOT6, remote sensing, FLAASH, algorithms, models

ACKNOWLEDGEMENTS

I must acknowledge and thank the Almighty God for his progressive provision, guidance and mercies that carried me throughout the course of this research. This thesis also owes its existence to the help, support and inspiration from several personalities.

First and foremost, I would like to express my sincere gratitude and appreciation to my supervisors Dr. Ir. Mhd. Suhyb Salama (1st) and Prof. Dr. Ing. Wouter Verhoef (2nd) for their guidance during this research work. I am heartily thankful to Dr. Ir. Mhd. Suhyb Salama for his tireless constructive critics, in-depth knowledge and advices as well as his motivation and encouragement throughout the thesis work. His immense support, especially helping me in writing codes in Matlab software to shape the application of the models/algorithms used in this study and also his inspiring suggestions have has been precious for the development of this thesis content. Am very grateful Dr. Salama and Prof. Verhoef. And also special thanks to Dr. Ir. C.M.M. Chris Mannaert for the laboratory setup and

I would like to thank the Vechtstromen and Brabantsedelta Water Boards for their supports. In particular I am indebted to Arjan Segeren, Guido Waajen from the Brabantsedelta, Sjon Monnix and Leontien van der Molen from Vechtstromen and Bas Waanders, Park manager of Het Hulsbeek for providing the sampling boats and facilitating the field works. I would like to thank the Netherlands Space Office (NSO) for providing SPOT-6 images through the Satellite Data Portal.

Particular thanks also goes to the Dutch Government for funding my studies through the Netherlands Fellowship programme (NFP) which made it possible for me to follow this programme here in the Netherlands. This also, would not have been possible without my nomination by the University of Cape Coast, Ghana through the Department of Geography and Regional Planning, UCC.

Many thanks to Dr. Benjamin Kofi Nyarko, UCC and Dr. James Kweku Eshun, UCC for their immense support and mentorship and also to all the lecturers/staffs of the Department of Geography and Regional Planning, UCC, Ghana.

I am also very grateful to Dr. Amos T. Kabo-bah, of the University of Energy and Natural Resources, Ghana, for his advice, prayer, support and encouragement. I will obviously not forget my colleagues Mujeeb, Aristotle, Justin, Kingsley, Peter, Henock, Julinda, Ali and Nana Adwoa for their encouragement and support throughout the challenges and tough times during my stay in ITC and to the all staff/lecturers and all my class mates of the Department of Water Resources, ITC-UT, The Netherlands. Finally, I would like to express my sincere appreciation to my family (Emmanuel P. Owusu, Lucy Y. Owusu, Josephine Achia Asamoah, and Grace Prempeh) and my siblings for the unflagging love and motivation, prayers and unconditional support which contributed to my well-being.

Thank you all.

TABLE OF CONTENTS

LIST OF FIGURES

LIST OF TABLES

LIST OF ABBREVIATIONS AND ACRONYMS

Chl-a – Chlorophyll-*a*/ Chlorophyll-*a* concentration

CET – Central European Time

FLAASH- Fast-line-of-sight Atmospheric Analysis of Spectral Hypercubes

FLH – Fluorescence Line Height

GPS – Global Positioning System

IOP's – Inherent Optical Properties

MCI – Maximum Chlorophyll Index

MERIS – Medium Resolution

MODIS – Moderate Resolution Imaging Spectrometer

MSI – Multi-Spectral Imager Imaging Spectrometer

NDVI – Normalized Difference Vegetation Index

NDCI- Normalized Difference Chlorophyll Index

NIR – Near Infrared

Nm – Nanometres

NTU – Nephelometric Turbidity Unit

OLI – Operational Land Imager

R^2 - Coefficient of Determination

rMAE – Relative Mean Absolute Error

Rrs – Remote Sensing Reflectance

TIRS – Thermal Infrared Sensor

TOA – Top-of-Atmosphere

WQRS - Water Quality Remote Sensing

FBS/4BS – Four Band Algorithm

3B – Three band Algorithm

1. INTRODUCTION

1.1. Background

Inland water resources are becoming more prone to danger due to climate change and human activities (Majozi et al., 2014). Some deteriorating factors include rapid development as well as industrialization and urbanization which have occurred around many inland waters in the past few decades (Feng et al., 2014).

Photosynthetic algae support healthy aquatic ecosystems by fixing carbon and producing oxygen which help in creating the base of the food web. However, under certain circumstances, some species can form high-biomass and/or toxic productions of cells or blooms, thereby causing harm to aquatic ecosystems (plants species and animals) and to humans through direct exposure to water-borne toxins or seafood consumption (Kudela et al., 2015). Damage caused by high-biomass blooms to ecosystem may include, for example, food webs damage, fish-kills, or low oxygen dead-zones after bloom degradation. Some species also produce dominant natural chemicals (toxins) that can persist in the water or enter the food web, leading to illness or death of aquatic animals and even human though seafood consumers (Heisler et al., 2008; Kudela et al., 2015). In addition, with the persistent reduction in the availability of water resources due the impact of total algal biomass or simply put, eutrophication which is a major water quality problem affecting many shallow aquatic ecosystems, the protection and maintenance for supporting water quality has become a primary objective of most water resources management (Huang et al., 2010).

Chlorophyll-*a* as an essential pigment of the algae family is normally used to determine the biomass and productivity status of phytoplankton in aquatic systems. Chlorophyll-*a* concentrations on the other hand, shows the degree of eutrophication in water (Tian et al, 2014).

The presence of the overabundance of these phytoplankton blocks the direct sunlight from reaching the lower layer of waters, therefore depriving aquatic life the essential sunlight needed for its growth. This causes severe depletion of dissolved oxygen in waters and fatally affects aquatic life and causes many respiratory disease and skin disorders in human too (Teneva et al., 2010; Moreira et al., 2014). Therefore there is a paramount need for early detection, prediction and quantification of these algal bloom.

There are lack of comprehensive methods for monitoring and estimating Chlorophyll-*a* concentration in small inland water bodies. This problem will be addressed by employing empirical models using Landsat-8 and/or SPOT-6 Multi-Spectral data as well as concurrent in-situ measurements. In this research, we will inter-compare different algorithms or models and adapt the most accurate one to derive Chlorophyll-*a* (Chl-*a*) from Landsat-8 Operational Land Imager (OLI) or SPOT-6.

1.2. Problem Definition

Most existing techniques that are common for estimating the presence of Chlorophyll-*a* (Chl-*a*) as a proxy for total biomass blooms in small water bodies are in-situ sampling. This technique has its own disadvantages, that is, neither the spatial nor the temporal frequency is sufficient to detect the extent and intensity of algal blooms in water bodies. Therefore, field sampling is seen to be very laborious and time consuming and may come with inaccurate measurements and uninterpretable results (El-Alem et al., 2012). Inland waters are small water bodies that are not detected by current ocean color satellites, example, Moderate Resolution Imaging Instrument (MODIS) ~1000m. On the other hand, multispectral satellites, such as Landsat-8 and SPOT6, with a spatial resolution of approximately ~10m to ~30m and ~1.5m to ~6m respectively will provide the required spatial resolution to detect these small water bodies.

Traditionally, most Chlorophyll-*a* (Chl-*a*) models were developed for the clear ocean water and ocean color satellites. In this research, we will investigate the opportunities of Landsat-8 and SPOT6 to estimate Chlorophyll-*a* (Chl-*a*) in inland waters. The lack of comprehensive methods for monitoring and estimating inland waters eutrophication problem such as Chlorophyll-a concentration will be addressed by using inter-comparisons of models/algorithms with respect to Landsat-8 or SPOT-6 Multi-Spectral sensor and concurrent field measurements.

1.3. Research Objectives

The objective of this research is to identify and adapt a model that is suitable for quantifying or estimating Chlorophyll-*a* (Chl-*a*) from inland waters from multi-spectral data in Lakes Binnenschelde, Markiezaatsmeer and Hulsbeek.

1.4. Research Questions

The research questions that will be answered in this research based on the following:

a. How can we adapt a model such that it can use Landsat-8-OLI and SPOT-6 to estimate Chl-a (chlorophyll-a absorption) and produce validated Chl-*a* output maps?
b. Which model (based on performance) is best for the quantification and detection of Chl-*a* in inland waters for the specific study areas?
c. How much error do Landsat-8-OLI and SPOT-6-MSI multi-spectral setup introduces to the derivation of Chl-*a*?
d. What is the gained knowledge of having high resolution maps from Landsat-8 and/or Landsat-8-OLI and SPOT-6?

1.5. Purpose of the Study

Remote sensing is considered as one of the effective water quality monitoring techniques in the retrieval of Chlorophyll-*a* (Chl-*a*) for water bodies (Matsushita et al., 2015). By the end of this research, the relevance in the application of Landsat-8-OLI or Spot-6-MSI satellite in monitoring, estimating and quantification of

Chlorophyll-*a* (Chl-*a*) using different models (algorithms) will be realized. Hence executing and developing an efficient remote sensing method of quantifying the amount of Chl-*a* in Lakes Binnenschelde, Markiezaatsmeer and Hulsbeek.

1.6. Structure of Research

The structure of this research work include Chapter 1 which introduces the general description of the work. It also describes the problem definition, research objectives, research questions as well as added values. Chapter 2 outlines the literature review and explains some basic concepts of chlorophyll-a, remote sensing of environment and chlorophyll-a estimation algorithms. Chapter 3 outlines the study area and data collection procedure. In Chapter 4, the methodology is explained. Then in Chapter 5, the results of the field measurements and simulated/convolved data for estimating Chl-a in different scenarios with four models will be presented. This include the application and validation of the models. Chapter 6 will contain the discussion and analysis of the results while Chapter 7 make the conclusion and recommendations. Finally, Chapter 8 will end the research work with references and appendices. The elements of this research will take the form as illustrated below in figure 1-1.

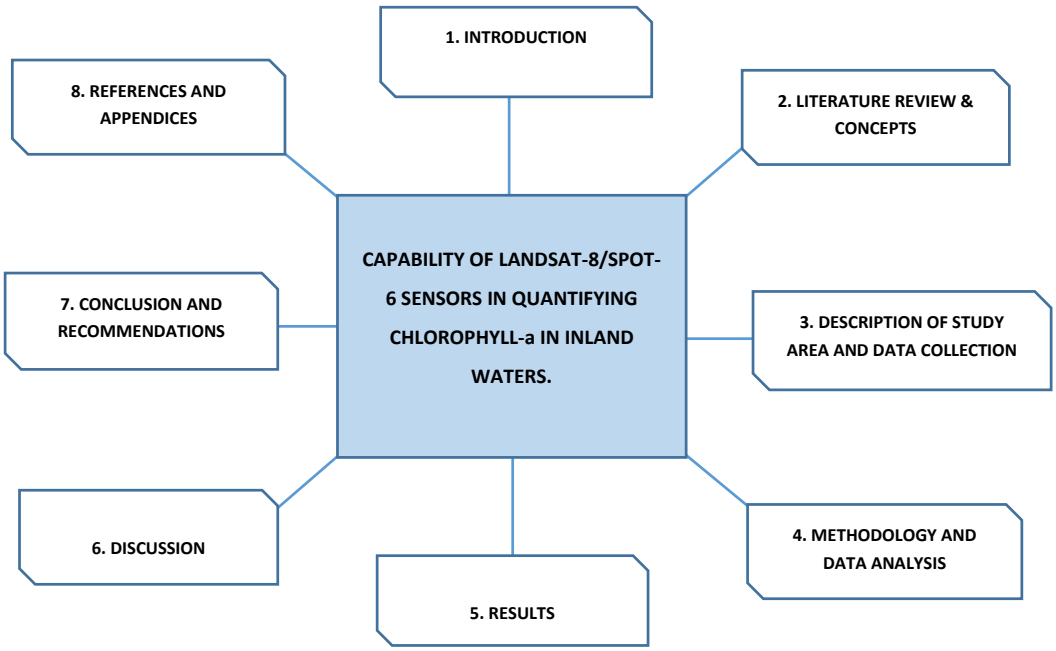

Figure 1-1: Structure of Research to be undertaken (Author Construct, Owusu, 2015).

2. LITERATURE REVIEW

2.1. Chlorophyll-*a* caused through water eutrophication

One of the major drivers of eutrophication and development of harmful algae (shown in figure 2a&2b) has been attributed to nutrient pollution (Lapointe et al, 2015). Chlorophyll-a is the green pigment responsible for photosynthesis that exists in all phytoplankton classes (Watanabe et al., 2015). In recent years, eutrophication of water systems has become a problem worldwide and an in-depth understanding about water eutrophication will help reduce the phenomena of the growth of algae (Yang et al., 2008). Detecting and quantifying chlorophyll-*a* (Chl-*a*) is one of the most important indicator for evaluating the eutrophication status of a water body in time and space (Matsushita et al., 2015).

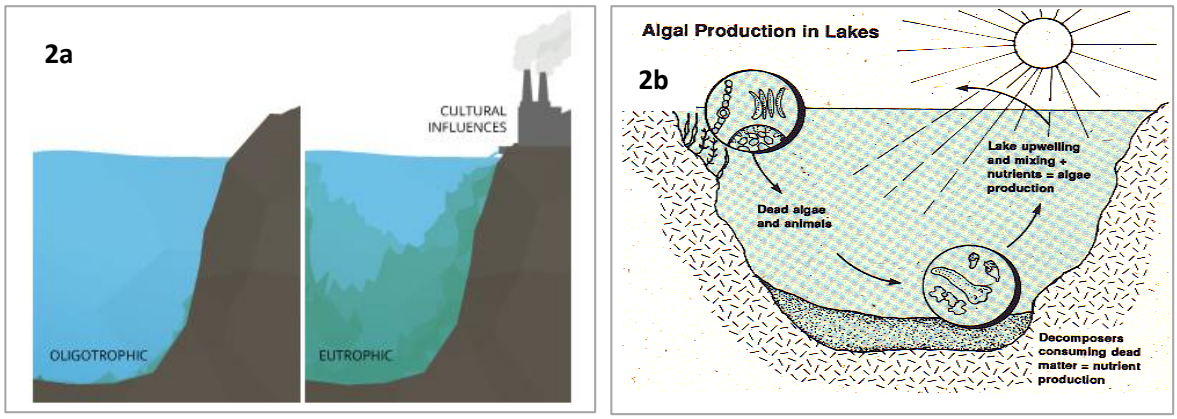

Figure 2-1a & 2-1b: Schematic process of eutrophication and formation of algae in eutrophic case 2 waters.

Photo source for Figure 2-1a & Figure 2-1b. (http://www.fondriest.com/environmental-measurements/parameters/water-quality/algae-phytoplankton-chlorophyll/) & (http://www.ecy.wa.gov/programs/wq/plants/management/joysmanual/chlorophyll.html .

Chlorophyll-*a* (Chl-*a*) has been identified as one of the major ways of knowing the phytoplankton biomass and bio-production in various water bodies (Kutser et al, 2005). Chlorophyll-*a* (Chl-*a*) which also a proxy of photosynthetic algae can be harmful to human health (Huang et al., 2010). Estimating chlorophyll-*a* in water will help in understanding the status: the physical and bio-chemical components of water are of keen interest to the researcher and policy makers respectively (Palmer et al., 2015).

According to literature, for many decades, satellite remote sensing of water quality has been undertaken typically for open ocean and coastal waters which provide information of the status of water based on primary production, suspended particulate matter, non-algal particles, coloured dissolved matter (CDOM) and chlorophyll-a as an indicator of total phytoplankton biomass. (Cui et al., 2010). Normally, most phytoplankton (Photosynthetic algae) have smaller impact in multi-spectral remote sensing because most

phytoplankton are very small to see with the naked eye. However, some types of blooms may be noticeable due to the large presence of chlorophyll-a (Chl-*a*) as it appears as coloured pigments on water surface. The abundance and spatial distribution of phytoplankton in waters through the use of remote sensing techniques to estimate Chlorophyll-*a* (Chl-*a*) has relied mostly on algorithm (Kamerosky et al., 2015). However, remote sensing of water quality of small water bodies has been hindered by the course spatial resolution of available ocean colour sensors (Groetsch et al., 2014). This makes it unconducive in the application over small inland water bodies such as lakes, lagoons, rivers, reservoirs among others (Rantajärvi et al, 1998). Although, current multispectral sensors have the required spatial resolution to map small water bodies, they do not have the required spectral characteristics (resolution) for many water quality applications (Berni et al., 2009).

2.2. Remote Sensing of Chlorophyll-*a* in Open Waters

Using remote sensing to precisely estimate Chl-a pigment (phytoplankton) in turbid productive waters is mostly difficult (Yi et al., 2013; Zimba & Gitelson, 2006). However, satellite remote sensing based on red and near-infrared wavelengths has proven to be very useful in observing chlorophyll-a concentrations (Chl-a) in water bodies (Yu et al., 2014). Based on spectral characteristics of water, Chl-a concentrations can be mapped through remote sensing images by means of quantitative retrieval methods. Chlorophyll-a has an approximate absorbance maxima of around 430 nm and 662 nm. By measuring the absorption of light in the red and NIR regions, it is possible to estimate the concentration of chlorophyll-a.

The ease of using remote sensing to quantify and estimate Chl-*a* in open waters depends primarily on the optical properties of the water body under study. Basically, high spatial and temporal resolution data can be derived from most multispectral satellite and airborne optical sensors for monitoring and estimating inland and coastal water ecosystems (Gitelson et al., 2008).

In general, algorithms (empirical/semi-empirical) that uses the blue and green spectral channels can be used to derive comparatively accurate chlorophyll-*a* concentration in open case-1 waters. This is because open case-1 waters generally uses spectral responses in the blue and green channels and are influenced only by phytoplankton (O'Reilly et al., 1998). However, in case-2 waters, the application of the blue-green spectral channels is not reliable for the estimation of chlorophyll-*a*. This is because reflectance (Rrs) in these spectral regions do not provide a clear and reasonable correlation between Chl-*a* and other water constituents including absorption by Coloured dissolved organic matter (CDOM), Total Suspended Material (TSM) and other non-algal particles in productive turbid waters (Darecki et al., 2004; Dall'Olmo et al., 2005). Remote sensing reflectance (Rrs) at these wavelengths are not only affected by phytoplankton but also affected by other water constituents such as CDOM, Non-Algae Particle (NAP), and Total Suspended Materials (TSM) which is attributed to the strong absorption properties of these particles in the visible spectral channels (Gitelson et al., 2008).

Some previous studies suggested that, estimating chlorophyll--*a* in most turbid productive waters is necessary along the red and near-infrared spectra domain (Dall'Olmo et al., 2005). Such estimation in turbid

productive waters presents a number of challenges, largely due to the complexity of turbid waters. Also, it is difficult to obtain high quality satellite images for a specific time and locations because of the limitation of the satellite revisit period and atmospheric conditions(Tian et al., 2014). In the principles of band ratios, the most bands associated with Chlorophyll-*a* estimation (in both case I and case II) include the blue, green, red and near-infrared bands. Normally, two spectral bands are selected for the estimation of Chlorophyll-a (Gitelson et al., 2000). Consequently in the case of chlorophyll-a, one band corresponds directly to high reflectance and one band corresponds to high absorption. Hence, the use of remote sensing data is viable alternative for mapping Chl-a pigments (Watanabe et al., 2015).

2.3. Algorithms for Estimation Chlorophyll-*a*

Most empirical and semi-analytical models or algorithms have been developed to use coincident in-situ chlorophyll-*a* and remote sensing reflectance (Rrs) and are easy and straightforward to use for data processing (IOCCG, 2006). The development of many empirical algorithms for the estimation of chlorophyll-*a* were based on the spectral properties of inland turbid productive waters. The MCI, N3B, NDCI, and 4B empirical algorithms, shown in table 2-1 and originally developed and proposed by (Gower et al., 2008), (Gitelson et al., 2008), (Mishra & Mishra, 2012) and (Le et al., 2009), were employed in this studies for the estimation of chlorophyll-*a* which are mostly based on red and near-infrared (NIR) spectral channels. They have proven to be a good indicator for retrieving chlorophyll-*a* in most eutrophic inland waters (Watanabe et al., 2015). Most of the algorithms used in this study are have a direct one step empirical relationship with chlorophyll-*a*. However, the application of these algorithms on the dataset used in this study will prove whether the aforementioned bands/spectral channels are good in estimating Chl-a.

Gower et al., (2008) suggested that the MCI model allows for the estimation of Chl-a inland productive waters using the red and infrared bands aiming at the red-edge signatures that are linked to Chl-*a* and its florescence line height. Binding et al ,(2013) also stated that MCI product has proven to be a versatile tool in the monitoring algal bloom in most turbid productive waters of chlorophyll-*a* >10 $mg.m^{-3}$. In general, these algorithms were analyzed against laboratory measured absorption of pigments and Trios-Ramses-ACC derived reflectance as well as Landsat-8/SPOT-6 derived reflectance.

The objective of this research is to identify and adapt a model that is suitable for estimating Chlorophyll-*a* (Chl-*a*) concentration in inland waters from multi-spectral data on Lake Binnenschelde, Markiezaatsmeer and Hulsbeek using least squared regression and statistical accuracy methods. However, the performance of models used in deriving Chl-a is subject to compatibility between the type of data used and the type of waters under study (IOCCG, 2006).

Table 2-1: An overview of algorithms to derive or estimate Chl-*a.* (Chl-a absorption coefficient)

Model Abbreviation	Algorithm Equations/Band Combination.	Author
MCI	$\mathbf{C_{pigm}} = (Rrs\lambda_1) - (Rrs\lambda_2) * \frac{(\lambda_2 - \lambda_1)}{(\lambda_2 - \lambda_1)} * (Rrs\lambda_3) - (Rrs\lambda_1)$ where; λ_1=665, λ_2=709, and λ_3=753	(**Gower et al., 2008)**
3B	$\mathbf{C_{pigm}} = [(Rrs^{-1}(\lambda_1) - (Rrs^{-1}(\lambda_2)] * Rrs(\lambda_3)$ where; λ_1=665, λ_2=709, and λ_3=753	**(Gitelson et al., 2008)**
NDCI	$\mathbf{C_{pigm}} = \frac{[(Rrs\ (\lambda_2) - (Rrs(\lambda_1)]}{[(Rrs\ (\lambda_2) + (Rrs(\lambda_1)]}$ where; = λ_1=665 and λ_2=708	**(Mishra & Mishra, 2012)**
4B (FBS)	$\mathbf{C_{pigm}} = [(Rrs^{-1}(\lambda_1) - (Rrs^{-1}(\lambda_2)][(Rrs^{-1}(\lambda_1) - (Rrs^{-1}(\lambda_2)]^{-1}$ where; λ_1=663, λ_2=693, λ_3=709 and λ_4=740	**(Le et al., 2009)**

where λ_1, λ_2, λ_2, λ_3 and λ_4 are reflectance bands that the sensor receives at a specific wavelength.

3. DESCRIPTION OF STUDY AREAS AND DATA COLLECTION

3.1. General Description

The study areas for this research comprises of three (3) lakes namely; Lake Markiezaatsmeer, Lake Binnenschelde and Lake Hulsbeek, all located in The Netherlands. Water quality of these three (3) study areas are mainly endangered by agricultural runoff as well as pollutant point source from water treatment plants since the surrounding land is largely used for agricultural and water treatment purposes. Climatic impact and increased in the decomposition of sediments has led to internal eutrophication (van Dam & Mertens, 2013). Previous research indicated that there have been incidence of growth of algae bloom in such lakes in the Netherlands and this poses health risk on aquatic life and humans as well in relation to water quality. Hence, it was based on this that the study areas were specifically chosen for this research.

3.1.1. Geographical Characteristics of study areas: Lakes Markiezaatsmeer, Binnenschelde and Hulsbeek.

Lakes Markiezaatsmeer, and Binnenschelde are smaller inland lakes. Both lakes Markiezaatsmeer and Binnenschelde are located on same latitude 51°29´N and but different longitudes. Lake Binnenschelde lies on longitude 4°17´E while Lake Markiezaatsmeer also on 4°16´E respectively. However, Lake Hulsbeek lies on latitude 52°18´N and longitude 6°53´E. Descriptive characteristics of the three study areas are described in table 3-1 below. They serve as a major water reserves for drinking water and for agricultural purposes. These lakes are used for transportation, fishing, sand mining, wind energy generation and also for water sport. In addition, Lake Hulsbeek, which also a small inland lake is found in Hulsbeek area which is one of the top recreational area in the Province of Overijssel. It has a total area of about 250,000 hectares. The lake consist of a swimming pond and a fishing pond with some skate board ramps located in it. Map of locations of these study areas are presented in figures 3-1 to 3-3.

Table 3-1: Summary of Location(s) and characteristics of the three (3) study areas.

Study Area	Latitude : Longitude	Average Depth (m)	Max. Depth (m)	Surface Area (km^2)	Trophic Status	Topography
Lake Binnenschelde	51°29´N **:** 4°17´E	1.5	3.5	1.78	Eutrophic	Predominantly flat
Lake Markiezaatsmeer	51°29´N **:** 4°16´E	2.1	3.0	21.9	Eutrophic	Predominantly flat
Lake Hulsbeek	52°18´N **:** 6°53´E	-	6	2.5	Eutrophic	Predominantly flat

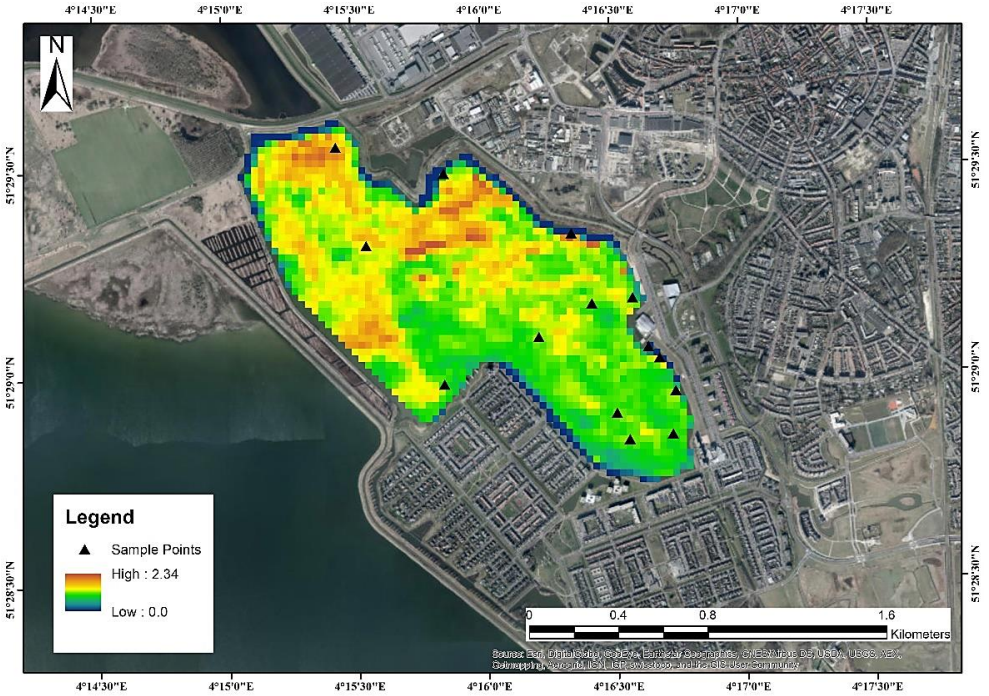

Figure 3-1: Landsat-8 image of Lake Binnenschelde displaying the locations and sample points from a Chl-a absorption map collected on 23rd of September, 2015.

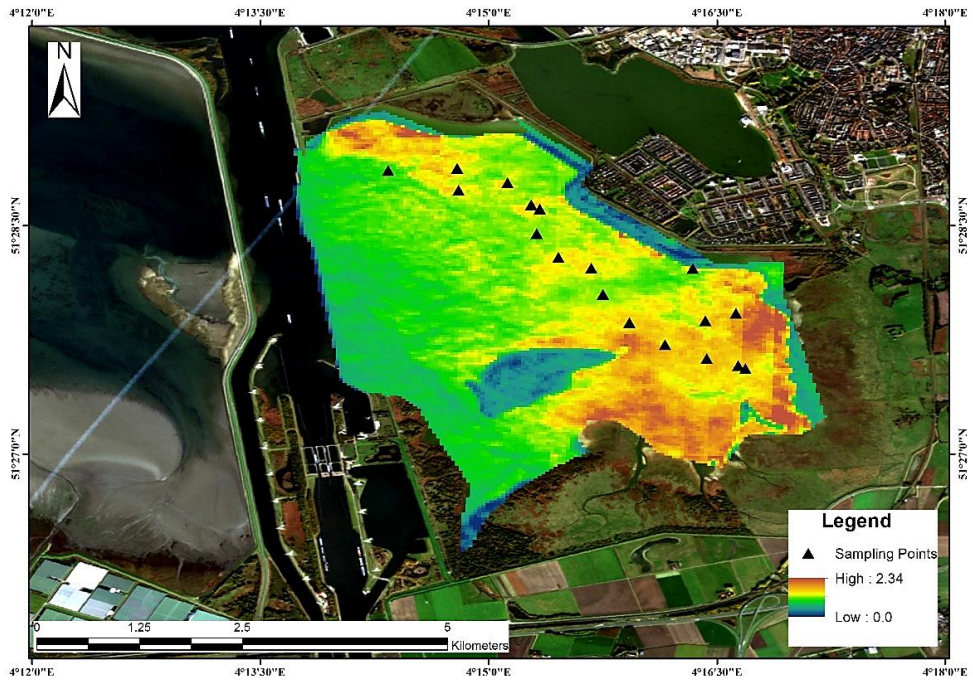

Figure 3-2: Landsat-8 image of Lake Markiezaatsmeer displaying the location and sample points from a Chl-a absorption map collected on 27th of September, 2015.

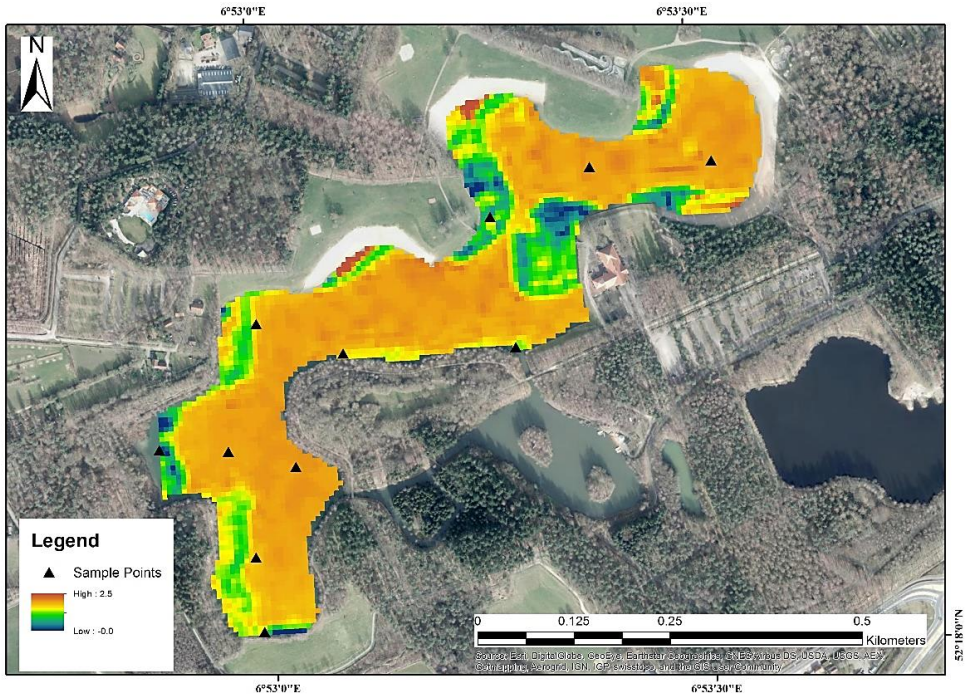

Figure 3-3: Landsat-8 image of Lake Hulsbeek displaying the location and sample points from a Chl-a absorption map collected on 26th of September, 2015.

All images (figures 3-1 to 3-3) above, were showed in resulted chlorophyll-aabsorption maps with its surroundings in true colour and the black triangle symbols indicates the sampling points from each of the lakes.

3.2. Datasets

As discussed in section 3.1, three lakes in The Netherlands were considered in this study: Lake Markiezaatsmeer, Lake Binnenschelde and Lake Hulsbeek, with surface areas of 21.9 km², 1.78 km² and 2.5 km² respectively (table 3-1: fifth column). Intensive field data collection protocols were observed for Lakes Markiezaatsmeer, Binnenschelde and Hulsbeek during a cruise using a boat. All data from these three (3) different sites were processed and used in this study. At these three sites, all in different basins, radiometric measurements were taken. Surface water samples were also collected and returned to the laboratory for processes and analysis of Chl-a concentrations, absorptions due to phytoplankton pigments and CDOM and among other concentrations. However, Landsat-8 and SPOT-6 images were also downloaded simultaneously for match up and further analysis.

3.2.1. Remote Sensing Data (Images) of the Study Area - Landsat-8-OLI/SPOT-6

Different Landsat-8 and SPOT-6 scenes which comprises 11 and 4 bands were downloaded from USGS_Earth_Explorer center (USGS website) using this http protocol: (http://earthexplorer.usgs.gov/). The landsat-8 has a pixel size of 15/30/100 meters while SPOT-6 is also in 1.5/6 meters respectively and the bands for each sensor are acquired simultaneously. These multispectral imagery data were acquired between the dates of 1st April and 31st December, 2015 over Lakes Markiezaatsmeer, Binnenschelde and November to December, 2014 and 2015 for Lake Hulsbeek. The properties and characteristics of the level 1T landsat-8 and SPOT6 products which are in HDF format are listed below:

LANDSAT-8

- ✓ Launched Date – February 11, 2003
- ✓ Sensor Accuracy - OLI - 12 m & TIRS - 41 m circular error (all with 90% confidence)
- ✓ Data type and output format - 16 bit produced in GeoTiff format
- ✓ Image Orientation and Projection – North-up with a UTM projection
- ✓ Ellipsoid – WGS84

The properties of the level 1T SPOT-6 product which are also in HDF format are listed below:

SPOT6

- ✓ Launched Date – September 9, 2012
- ✓ Sensor Accuracy - 35 m & 10 m circular error (all with 90% confidence)
- ✓ Data type and output format - 12 bit also produced in GeoTiff format
- ✓ Image Orientation and Projection – North-up with a UTM projection
- ✓ Ellipsoid – WGS84

(USGS, 2013).

Table 3-2: Landsat-8 (MSI)-OLI + TIRS spectral bands designations.

Spectral Ranges	Wavelength (µm)	Central Wavelength (nm)	Resolution (m)
Band 1 - Coastal aerosol (OLI)	0.433 - 0.453	443	30
Band 2 – Blue (OLI)	0.450 - 0.515	482	30
Band 3 – Green (OLI)	0.525 - 0.600	562	30
Band 4 - Red	0.630 - 0.680	655	30
Band 5 - Near Infrared (NIR) (OLI)	0.845 - 0.885	865	30
Band 6 - SWIR 1 (OLI)	1.560 - 1.660	1610	30
Band 7 - SWIR 2 (OLI)	2.100 - 2.300	2200	30
Band 8 – Panchromatic (OLI)	0.500 - 0.680	590	15
Band 9 – Cirrus (OLI)	1.360 - 1.390	13372	30

(USGS, 2013; Survey, 2015 and Barsi et al., 2014).

Table 3-3: Spot 6 spectral bands designations.

Spectral Ranges	Wavelength (µm)	Resolution (m)
Band 0 - Blue	0.430 - 0.550	6
Band 1 – Green	0.530 - 0.590	6
Band 2 – Red	0.600- 0.695	6
Band 3 – Near Infrared	0.760 – 0.890	6

Table 3-2 and 3-3 shows the spectral band properties of both Landsat-8 OLLI/TIRS and SPOT6. The spectral response properties of any sensor likewise landsat-8 and SPOT is vital to understand in terms of exploiting its data (Barsi et al., 2014). The shaded band designations were used in calculating Chl-*a* (Chl-a absorption) based on the four (4) models used. These bands, mostly the red-NIR, were chosen because of their sensitivity and high potential in estimating Chl-a (Yu et al., 2014).

3.2.2. In-Situ Measurements

Two datasets including ground truth radiometric reflectance data and Chl-*a* concentration (Chl-*a*) data were used in this study. These include radiometric data and water samples that were collected from each of the sites. Both radiometric measurements (above-water and in-water) were taken to estimate and analyse the spectral reflectance characteristics for each lake.

However, radiometric measurements, both radiance and irradiance measurements, above and below water surface (in figure 4-2) were carried out on the site in the case of Markiezaatsmeer, Binnenschelde and Hulsbeek in September (23rd, 24th and 26th September, 2015 respectively) using the Trios RAMSESARC and RAMSESACC-VIS sensors. For minimal effect of clouds, measurements were taken between the hours of 11am and 15:10pm CET. Table 4 below shows the number of radiometric measurements (bio-optical parameters), water samples and time for sampling. In all, the Trios RAMSES-ARC measured upwelling radiance signals Lu (λ0) and Trios RAMSES-ACC-VIS measured down-welling irradiance signals Ed (λ0+) between a wavelengths of 300 nm to 900 nm (in the case of this study).

Table 3-4: Number of radiometric measurements and water samples taken and time for sampling.

Sampling Area Location and Dates	Sampling Time (All time in CET)	Number of points for Radiometric measurements (N)	Number of water samples (n)
Lake Binnenschelde (23rd September, 2015)	From 11:50am -15:05pm	10	4
Lake Markiezaatsmeer (24th September, 2015)	From 12:05am -15:10pm	15	6

Lake Hulsbeek (26th September, 2015)	From 12:05am -15:10pm	11	6
Total	-	36	16

Source: (Author Construct, Owusu, 2016).

Table 3-4 above describes the date and time of sampling, number of radiometric measurements made and the number of water samples collected from each lake. The largest sample size was in Lake Markiezaatsmeer (N=15) while the smallest sample was in Lake Binnenschelde (N=10). It is important to note that laboratory analysis was done in addition to the radiometric measurements and used in evaluating the ability of the selected models in quantifying and estimating Chlorophyll-a by comparing true ground data (in-situ observations with derivatives of Chl-a by each models. Each study area location, measurements and sampling locations were geographically recorded using GPS mapping device. Table 3-5 shows the parameters measured on the field campaigns. A Chl-a absorption overlay on a true colour composite image of the study area is also shown in figures 3-1 to 3-3 above in section 3.1.1. The water status and measurement protocols followed in Lake Binnenschelde, Markiezaatsmeer and Hulsbeek are also shown in appendix c.

In general, the colour observed in the lakes Binnenschelde, Markiezaatsmeer and Hulsbeek in the figure in appendix b, was mostly green. This give an indication that these lakes are eutrophic in nature. It also shows the radiometric set-up including micro-flu sensors for radiometric measurements using the Trios- RAMSES radiance and irradiance sensors.

Table 3-5: Field Parameters and Measurement details.

Parameters for Radiometric Measurements			Laboratory Water Samples	
Above Water	**SI Units**		**Laboratory Analysis**	**SI Units**
Upwelling Radiance Lu (λ)	$W\ m^{-2} sr^{-1}$		CDOM	m^{-1}
Downwelling Irradiance $Ed^{+}(\lambda)$	$W\ m^{-2}$		Chlorophyll-a concentration	$mg.m^{3}$
Below Water			Turbidity	NTU
Downwelling Scaler Irradiance $Ed^{-}(\lambda)$	$W\ m^{-2}$		Absorption coefficient of Chl-a pigments	m^{-1}
Sky Radiance Lsky (λ)	$W\ m^{-2} sr^{-1}$		Others: Temperature	°C

Details of measurements and parameters measured on the field campaign with its symbols and units are presented in Table 3-5 above. The processes involved in data sampling during and after the data collection is also shown in the Methodology flow chart in appendix b.

3.2.2.1. Water Samples (Laboratory Measurements for deriving Chlorophyll-a concentrations).

Water samples that were collected during the fieldwork at the same time the radiometric data were also acquired covered a wide range of biogeochemical and optical variabilities in these inland waters. Samples that were collected at each sampling site were stored in the fridge for some few days and then further analysed for their concentrations at the ITC - University of Twente laboratory. Analysis of water quality parameters included Chl-a concentration ($mg.m^{-3}$) as well as spectral absorption coefficient for Chlorophyll-a/phytoplankton pigments ($m.^{-1}$). Moreover, absorptions coefficients of Suspended Particulate Matter (SPM) and Total Suspended Materials (SPM) and Coloured dissolved Organic Matter (CDOM) were also analysed at the laboratory with their units in $m.^{-1}$. Simple filtration method was executed for the extraction of absorption coefficients Chl-a/phytoplankton pigments using 90% acetone and measuring its absorbance and transmittance in a VW-UV-VIS-3600-PC Spectrophotometer. This is practically discussed in section 4.3.2 and 4.3.3 respectively.

3.2.2.2. Sampling Sites

Location and coordinates of sample sites are presented in Appendix a. The tables in appendix 1 shows accurate location of sample sites and their corresponding coordinates and time intervals in Lake Markiezaatsmeer and Binnenschelde as well as Hulsbeek. Sampled points codded as MK-S, BN-S and HL-s means Markiezaatsmeer sample, Binnenschelde sample and Hulsbeek sample and this is presented in Appendix A.

4. METHODOLOGY AND DATA ANALYSIS

This chapter discusses the various methods and acquisition of date that used to achieve the objectives of this study. Remote sensing and GIS are the major tools that were utilized and used to process images acquired from both Landsat-8 and SPOT6 satellites. Chapter 4 also discusses how data (water samples, radiometric measurements and images) were processed. The steps taken and the processes involved in the collection and analysis of the various datasets are explained in detail below.

4.1. Introduction

This study aim at using an empirical/semi empirical method/algorithms to estimate Chlorophyll-*a* concentrations (a_phy) in inland lakes in the Netherlands. The methodology used to achieve the objectives and answer the questions of this research is divided in three (3) parts. The first part is to know the spectral reflectance of the various water bodies which will help in validating the optimal wavelengths for each model/algorithm used in estimating chlorophyll-*a* as proposed by in table 2-1, and secondly to dispose Landsat- 8/SPOT-6 imagery with an approved and accurate atmospheric correction method to be able to apply the models and/or algorithms from spectral characteristics generated from the behaviour of the various lakes (water bodies) and also to determine how much error that Landsat-8/SPOT-6 introduce to the derivation of Chl-*a* and finally producing map of Chl-*a*. The overall methodology which is shown in the flowchart in appendix 4 below is to determine the best Chlorophyll-*a* estimation models/algorithms and then applying that best model to corrected Landsat-8/SPOT-6 maps (images). In this study, convolution of data was done before application of the models to images.

4.2. Proposed Approach

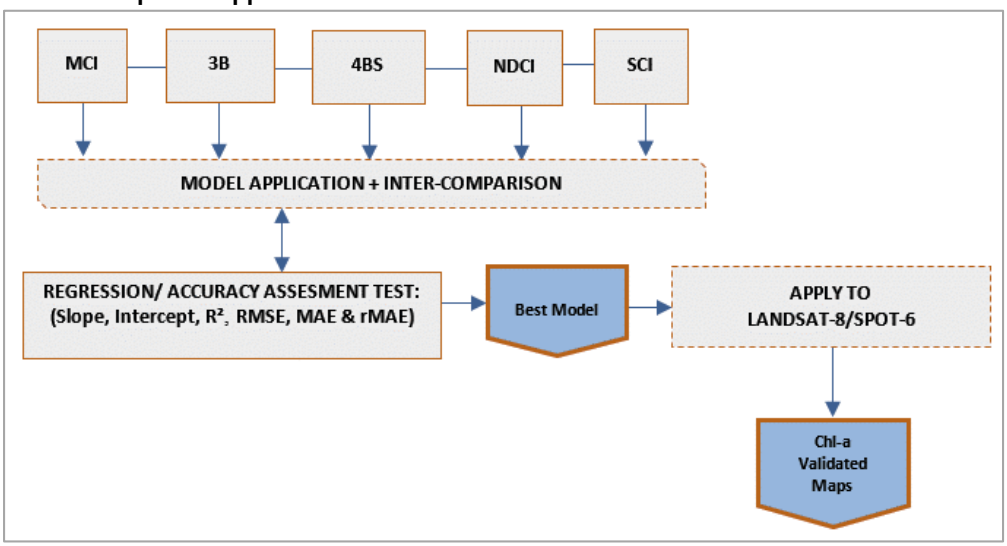

Figure 4-1: General framework for proposed model/algorithm application approach.

4.3. Data Processing

One of the major procedures in every scientific research focuses on the analysis and processing of various dataset acquired to achieve the objectives of its study. In the case of this study, three different data sets were used. The overall data type used and a schematic procedure of data processing is shown in table 4-1 below and figure 6-1 in Appendix 2 respectively. Further sub-headings will dealt more into how these various datasets were processed to achieve the aim of this study.

Table 4-1: Data type, instrument for acquisition, and processing.

Data type	Data Description	Instrument/Sensor Used	Type of Data Processing
In-situ	Radiometric Measurements	RAMSES-Trios (ARC-VIS & ACC-VIS)	Convolution and conversion of Spectral Measurements with Landsat-8 image
	Water sample	VW-UV-VIS-3600-PC Spectrophotometer	Intensive Laboratory analysis of aCDOM, a_phy/pig etc.
	GPS Coordinates	Garmin GPS System	
Landsat-8/SPOT-6 Images	Remotely Sensed Image	Landsat-8 OLI/TIRS SPOT-6	Atmospheric Correction using FLAASH setup

4.3.1 Derivation of Remote Sensing Reflectance (Rrs) from Radiometric Measurements.

Radiometric data were measured using three (3) RAMSES spectro-radiometers; an irradiance sensor (ACC-VIS) and the other two (2) were radiance sensors (ARC-VIS) with 7° field-of-view. The ARC-VIS and the ACC-VIS RAMSES spectro-radiometers works within a wavelength range of 320 nm to 950 nm with spectral sampling of approximately 3 nm. This 3nm interval was downscaled to 1nm with Landsat-8 spectral response bands. This made it easy to apply the appropriate wavelengths to each model calculation.

Remote sensing of water relies on detecting the light signals that leaves the water surface and reaches a sensor on board a satellite (D'Sa, Miller, & Del Castillo, 2006). Remote sensing reflectance is related to backscattering and absorption. It can be also stated clearly that the obtained measurements of water-leaving radiance (L_u), and downwelling reflectance (E_d) was used to compute the above water surface remote sensing reflectance (Rrs) using equation 1, which could be similar to the normalized water-leaving reflectance of Landsat-8/SPOT-6 product after matchup. The empirical algorithms or models used in this study to quantify/estimate the Chlorophyll-a concentration all uses remote sensing reflectance as input for the retrieval of Chlorophyll-a. According to in-situ data collected for this research, we considered above water radiometric measurements and this was adapted for the determining the remote sensing reflectance (Rrs).

Hence, the remote sensing reflectance (Rrs) with a unit of inverse steradians (sr^{-1}) was calculated using (Mobley, 1999; Montes-Hugo et al., 2008) equation below;

$$\text{Rrs}\,(\lambda,\theta,\varphi) = \frac{L_u(\lambda)}{\text{E}_d(\lambda)}[\text{sr}^{-1}] \quad \text{(Eq. 1)}$$

From equation (1), the ideal calculation of remote sensing reflectance (Rrs) will be computed by dividing the measurements of upwelling water leaving radiance L_u (λ) with the downwelling irradiance E_d (λ) just above the water surface measured in inverse steradians (sr^{-1}) while λ is the wavelength. Apparently, the remote sensing reflectance as adapted from equation 1 will be applied to all the models used in this study. The Mobley's equation for instance does not allow for any influence on the underwater measurement (L_u) hence its application in calculating for above water remote sensing reflectance (Rrs). The research will depend on the value of Rrs from the field measurements and that from image data after an accurate atmospheric correction has been performed. This will help to define the best fit algorithms for the estimation chlorophyll-a pigment or concentration in the respective lakes base on these reflectance values.

4.3.2 Derivation of Chl-a Concentrations ($mg.m^{-3}$) and Absorption Coefficients of Chl-a pigments (440 nm) [$m.^{-1}$]

A secondary data from the laboratory analysis was used. A simple fluorescence technique for the extraction of Chlorophyll-a (Chl-a) from planktonic algal cells was performed on the water samples individually collected for Markiezaatsmeer, Binnenschelde, and Hulsbeek sites. The Chlorophyll-a concentrations extraction (Chl-a_X) from the laboratory were calculated using the extraction by acetone method from absorbance data by adapting the Jeffrey and Humphrey's Trichromatic corrected Chl-a equations stated below in equation (2).

Secondly, the amount of Chlorophyll-a is expressed as the absorption coefficient at wavelength between 440nm, 630nm, 664nm and 647nm obtained from spectrophotometric of filtered water sampling with pores size of 0.2um or 0.4um depending on the amount of particles in each of the individual lakes.

The concentration of chlorophyll a for each field sample ($Chl\ a_f$) was calculated using equation (3). First, the absorbance value at 750 nm was subtracted from the selected wavelengths (664nm and 665 nm) of the Eq. (2). Similar subtraction was done all the specific absorbance used in this study including absorbance at 440 nm. This was done to correct for the backscattering of any small particles or fine colloidal matter in the samples hence removing any background turbidity form water samples

The absorption coefficient of Chl-a pigment/phytoplankton (440) was measured in the laboratory from equation 4 below;

$$Chl - a_X = 11.85\,(abs\,664) - 1.54\,(abs\,647) - 0.08\,(abs\,630) \quad \text{(Eq. 2)}$$

$$Chl - a_f = \frac{Chl\ a_E \times Extract\ Volume\ (L)}{Sample\ Volume\ (L) \times Cell\ Length\ (m)} \quad \text{(Eq. 3)}$$

Where;

Chl-a_x = concentration (mg/m^{-3}) of chlorophyll a in the extract solution measured,

Chl-a_f =concentration of chlorophyll a for each field sample,

abs 664 = sample absorbance at 664 nm (minus absorbance at 750 nm),

abs 647 = sample absorbance at 647 nm (minus absorbance at 750 nm), and

abs 630 = sample absorbance at 630 nm (minus absorbance at 750 nm).

The spectrophotometric analysis for the measured spectral absorbance at selected wavelengths (440 nm) was then converted to absorption coefficients of pigments/phytoplankton using equation (4) below;

$$a\_pig(440) = 2.3 * OD_S(440) * \frac{S}{V} \quad \text{(Eq. 4)}$$

This is similar to (Cleveland & Weidemann, 1993) equation. And this was done preceding to the application of the empirical algorithms.

From equation 4, a_{pig} (λ) is the absorption coefficient of pigments- in the case of this study, a_{pig} (440 nm), 2.3 is the correction factor that converts base 10 to natural log, OD_S is the measured of the sample filtered, S is the filter clearance area, V is the filtered volume (Mitchell et al, 2000). The absorption coefficient of non-algal particulate (a_{NAP}) or tripton was determined similarly using equation 4. Hence, absorption of Chlorophyll-a pigment or phytoplankton absorption was derived from the difference between particle and non-particle approximations using equation 5 below (Huang et al., 2013 and Mitchell et al, 2000)

$$a_{pig(440)} = a_p - * a_{NAP} \quad \text{(Eq. 5)}$$

4.3.3 Derivation Absorption Coefficients of CDOM (m.-1)

Based on this research, absorption coefficient of CDOM was analysed to determine the correlation between Chl-a and other water constituents (CDOM). Regression analysis was performed to confirm that the lakes being studied in this research are truly case 2 water – productive turbid waters. This analysis is discussed in section 5.2 under results and discussion. The CDOM absorption coefficients were calculated from laboratory for each site using (Bricaud et al., 1981) equation as follows:

$$a_{CDOM} = 2.3 * \frac{A_{CDOM}(440\ nm)}{r} \quad \text{(Eq. 6)}$$

Where A_{CDOM} is the optical density at wavelength 440nm and r is the cell length in meters. This values was corrected for backscattering using 700 nm as a referenced wavelength (Bricaud et al., 1981). This was used to analyse the status of water in relation to absorption of Chl-a pigments and chlorophyll-a concentration. In section 5.1.2., CDOM was regressed against both Chl-a concentration and absorption coefficient of Chl-a to determine the status of the lakes under studies.

4.3.4 Landsat-8 OLI/SPOT-6 Image Processing

High spatial and moderate resolution imagery is more important in mapping chlorophyll-a in inland lakes. For this reason, the use of Landsat-8 OLI and SPOT-6 images seem to be more adaptive in this study. Different landsat-8 and SPOT-6 images were downloaded from USGS Earth Explorer website. The images of the study area were in downloaded level 1GeoTiff products using GloVis (Global Visualization tool) tool. The images are in the following properties as shown in table 4-2. As shown in figure 4-2 below, data acquired from remote sensing requires that solar radiation passes through the atmosphere before it is collected by the sensors. For further processing and analysis to be done using such images, there is a need to do an accurate atmospheric correction in able to remove the effects and influences of the atmosphere on the final validated chlorophyll-a maps or images.

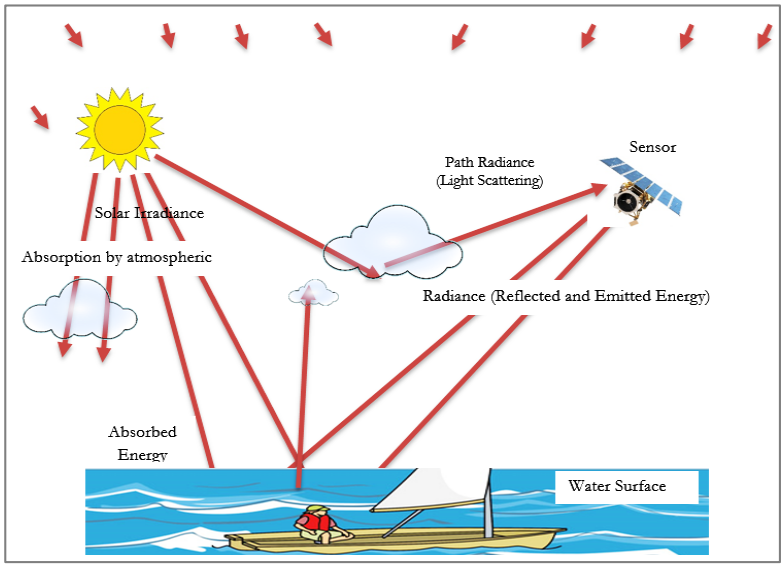

Figure 4-2: A schematic illustration of sun sensor pathway.

Figure 4-3 shows processes that contribute to the signal as measured by the sensor. It portrays the interaction of electro-magnetic radiation with the atmosphere and the Earth's surface). Source: Author's Construct (Owusu, 2016) and adapted from the ITC Core Book, 2013.

4.3.5 Atmospheric Correction of Satellite Images using FLAASH setup.

The necessity of monitoring water and deriving its optical properties requires a high atmospheric correction method and quantifying the contributions of aerosols and other atmospheric influences to TOA radiances (Vanhellemont & Ruddick, 2015). Similarly, Gordon et al., (1983) have indicated that the utmost step in estimating most water quality indicators is the derivation of water-leaving radiance (L_w) at their respective wavelengths (λ). Most atmospheric correction methods are image based and requires less or no external measurements (Vanhellemont & Ruddick, 2015). The derivation of radiances or reflectance information

from an image is only achieved through the application of an accurate atmospheric correction method. The effects of the atmosphere depends on the band or wavelength type and have distinct influence of the TOA reflectance (Bonansea et al., 2015). Most atmospheric correction method basically converts TOA radiance to water-leaving reflectance (TOA reflectance) and hence reducing errors or removing the effects of any atmospheric influences (Guanter et al., 2010). In this study, the fast line-of-sight atmospheric analysis of Spectral Hypercubes (FLAASH) atmospheric correction method which uses most Landsat-8 images as a case study, was applied on the two different satellite images: the first is Landsat-8 satellite images obtained on September 9th and 27th, 2015 and 3rd of August, 2015 for both Lakes Binnenschelde and Markiezaatsmeer as well as September 29th for Hulsbeek. The second set of images were SPOT-6 images which were also obtained on 2nd November and 4th December, 2015 for lakes Binnenschelde and Markiezaatsmeer as well as 3rd August and 27th July, 2015 for lake Hulsbeek. This is clearly listed in table 4-2 and 4-3 below. Some of these images comprises of errors which include noise, surface reflectance, aerosols, water vapour, solar irradiance curve as well as scattering and absorption influences. This may be due to changes in illumination angle, topology and instrument response among others. However, radiometric calibration and atmospheric correction were performed on these images to achieve the purpose of retrieving Chl-a concentration. This process was conducted using the ENVI Software Version 5.3.3. After performing radiometric calibration and atmospheric correction, DN values were converted to radiances (top-of-atmosphere radiances (L_{TOA} values) using the formula in equation 3. After obtaining the radiances from the image, a dimensionless top-of-atmosphere reflectance was then calculated using equation 4 and 5 respectively.

$$L_{TOA} = M_L Q_{CAL} + A_I \quad \text{..... (Eq. 7)}$$

where L_{TOA} is the top-of atmosphere (TOA) spectral radiance, M_L is the band specific multiplicative rescaling factor that is already in the image metadata of each of the study area, while A_l is the band specific addictive rescaling factor.

$$\rho TOA = \frac{\pi * L_{TOA*} d^2}{ESUN_\lambda * cos\theta_s} \quad \text{..... (Eq. 8)}$$

From equation 8, ρTOA is the dimensional top-of atmosphere reflectance, L_λ is the top-of atmosphere (TOA) spectral radiance at sensor, d is the Earth-sun distance in astronomical units, cos_θ is solar angle zenith angle in degrees as well as $ESUN_\lambda$ is the mean solar exoatmosphere irradiance for each band.

FLAASH setup was used as an atmospheric correction tool on the images acquired on Lakes Binnenschelde and Markiezaatsmeer. All the image data (Landsat-8 and SPOT-6) used in this study on which the atmospheric correction were processed using FLAASH setup. FLAASH setup corrects images for atmospheric interferences and simultaneously retrieves water quality variables without any tuning with field

measurements. Details of image data are specified below in table 4-2 and atmospheric correction processes are depicted in figure 4-4.

Table 4-2: Downloaded images for Landsat-8 OLI-TIRR for matchup.

Satellite Image Type and number of scenes	Landsat-8 data ID	Path- Row
Binnenschelde Bergen op zoom [a] Markiezaatsmeer [b], and (51.4876 N, 4.2648 E) [a] (51.4751 N, 4.2469 E) [b]	LC81980242015183LGN00.tar	P198 - R024
	LC81980242015215LGN00.tar	P198 - R024
	LC81990242015110LGN00.tar	P198 - R024
	LC81990242015158LGN00.tar	P198 - R024
	LC81990242015254LGN00.tar	P198 - R024
	LC81990242015270LGN00.tar	P198 - R024
Hulsbeek - 52.18 N, 6.53 E [c]	LC81970232015272LGN00.tar	P197 -R023

Table 4-3: Downloaded images for SPOT6-MSI for matchup.

Satellite Image Type and number of scenes	SPOT6 data ID
Binnenschelde Bergen op zoom [a] Markiezaatsmeer [b], and (51.4876 N, 4.2648 E) [a] (51.4751 N, 4.2469 E) [b]	MS_201512041016469_SEN_1608601101
	MS_201511011019559_SEN_1558406101
Hulsbeek - 52.18 N, 6.53 E [c]	MS_201508031011112_SEN_1403384101 MS_201406061017019_SEN_944881101

The accuracy of information obtained from each of the Landsat-8 and SPOT-6 images is dependent on the type of atmospheric correction method used. The in-situ reflectance spectra measurements taken for each lake were then with the corresponding derived Landsat-8 images reflectance after intensive atmospheric correction was performed. After atmospheric correction of images, only ROI's of Lakes Markiezaatsmeer, Binnenschelde and Hulsbeek were clipped out from the whole scene image and subjected to further processing. Again, the land around the lakes were mask out for proper analysis of the water properties.

4.3.6. Assumptions on selected bands and wavelengths for model application

The reflectance spectra is generally characterized by low reflectance at the blue and red region and high reflectance in the green, and in some cases the NIR regions. This study adapted four (4) algorithms including the Maximum Chlorophyll Index (MCI), New Three Band (N3B), Normalized Differential Index (NDCI), and the Four Band (FBS), which is mostly composed of ratios of red and near infra-red band as discussed in section 2.3.

There have been many studies that shows a close relationship between chlorophyll-a concentration and the Red-NIR ratios that is used to estimate chlorophyll-a in lakes (Dall'Olmo et al., 2005). Evidence shows that the 3B model could be utilized to derive chlorophyll-a concentration in turbid productive waters (Dall'Olmo et al, 2003). The 3 band (3B) model relates chlorophyll-a pigments to reflectance in the three spectral bands where λ_1 should be in the red range (670 nm), λ_2 should be in the range between 700-710 nm and λ_3 should be in the NIR around 700-750 nm (Dall'Olmo et al, 2003; Dall'Olmo & Gitelson, 2006).

However, there were some modifications in the band/wavelength selection for the models used in this study. Band shifting for the 700-710 range and the 730-753 NIR was performed to select the optimal band for each of the sensors. For instance, band 3, 4 and 5 were used respectively for Landsat-8; where λ_1 was maintained or fixed at 665nm in band 4, while the wavelengths λ_2 and λ_3 were tuned since they are not found in the Landsat-8 wavelength spectrum. In the case of this study, λ_2 and λ_3 were varied within the green band range and NIR band ranges respectively. Hence the Rrs at band 3 was selected for λ_2 at 708 nm while band 5 was selected for λ_3 which is also at 753 nm. Finally three wavelengths/bands were selected; Rrs at band 4 originally selected for λ_1 at 665nm, Rrs at band 3 selected for λ_2 at 708 nm and Rrs at band 5 selected for λ_3 at 753 nm respectively.

On the other hand, band 1, 2, and 3 were used for SPOT6 concurrently; where λ_1 was maintained or fixed at 665nm, λ_2 and λ_3 were selected from band 1 and band 3 respectively. Rrs at band 1 was selected for λ_2 and Rrs at band 3 was also selected for λ_3. This procedure was applied and repeated for all the models (MCI, 3B, 4B) - (see table c in appendix D). It should be noted that, this method was applied only for simulated or convolved Landsat-8 and SPOT6 data to select the optimal bands for the calculation and estimation of Chl-a (absorption of Chl-a). Direct wavelength application was however, used in relation to in-situ derived Rrs.

4.4. Simulation of Landsat-8 OLI and SPOT6 bands for Estimating absorption coefficients of Chl-*a* pigments.

Although the above mentioned models (in table 4-3) worked directly with field measured Rrs and concurrent Landsat-8 data, it could not work with SPOT6 data directly. Data simulation was performed on both Landsat-8 and SPOT6 using field measured reflectance (Rrs) to derive reflectance (Rrs) bands from Landsat-8 and SPOT6 data (Sun et al., 2015). Remote sensing reflectance (Rrs) from TRIOS RAMSES dataset was applied to spectral response of Landsat-8 OLI bands to simulate and resample bands to 1 nm spectral resolution.

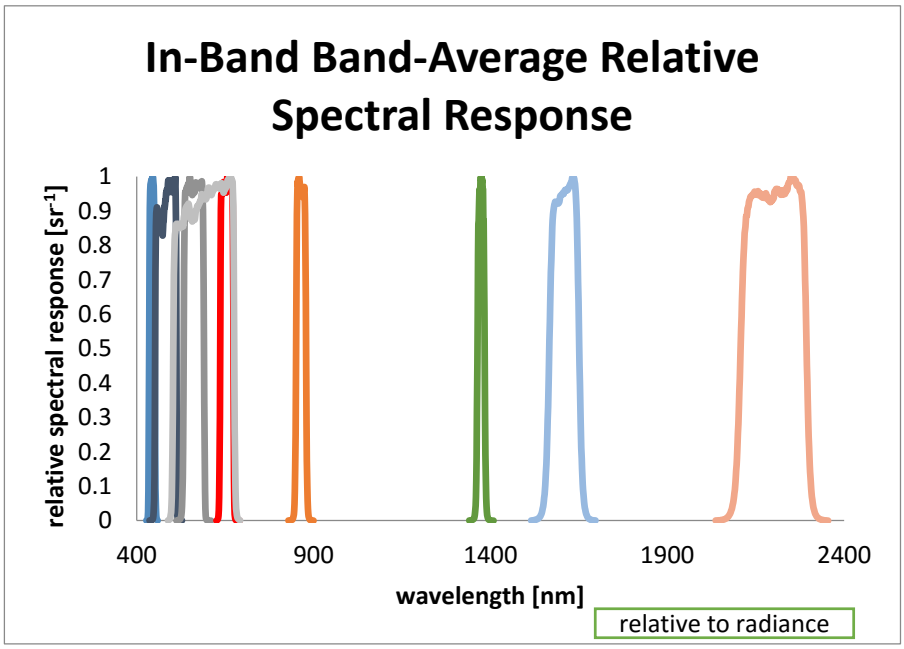

Figure 4-3: Landsat-8 OLI relative response functions.

Source of figure 4-5: http://pubs.usgs.gov/fs/2012/3072/fs2012-3072.pdf

The remote sensing reflectance (Rrs) of Landsat-8 OLI that were selected for estimating Chl-a from a model were convolved or simulated using Landsat-8 OLI spectral response (Barsi et al., 2014) and from landsat-8 website (http://landsat.gsfc.nasa.gov/?p=5779). The band average and its standard deviation is shown in appendix e. This was performed using Matlab software.

The optimal positions applied on field (in-situ) data is consistent with the finding of other researcher including the original authors of each model used in this study. However, different band tuning and selection was done for satellite data to find their optimal bands/wavelengths (see table 4-4 & appendix d). The selected bands for this research was based on the spectral characteristics of each lake discussed in section (5.3.) but a few band optimization was performed to adjust the traditional optimal bands to the type of sensor or data used. The MCI and 3B for instance, is sensitive and useful for the estimation of water chlorophyll. However, it requires three wavebands on 681, 709, and 753 nm (in some cases 665, 709, and 753 nm) whereas 709 and 753 are not available in the Landsat 8 product. In this case applied band shifting or band translation was used to select the optimal band from Landsa-8 bands to do calculations and estimation of modeled Chlorophyll-a in this study.

Since there is no wavelength column around 700 nm to about 830 nm for landsat-8 wavelength spectrum, the band selection and combinations procedure stated in table 4-4 and discussed in section 4.3.7 were used. Quiet a range of selection was done to find the optimal band that fit each of the algorithms used.
After simulation, the following bands combination in table 4-4 were chosen for the calculation of modelled chlorophyll-a. This was done after simulating Landsat-8 and SPOT6 spectral response function with field measured Rrs to derive Landsat-8 and SPOT6 derived Rrs. This help in selecting the right band for model application.

Table 4-4: Band combination for simulated data for Landsat-8 and SPOT6.

Model	Band selection Landsat-8	R^2	Band selection SPOT6	R^2
MCI	3, 4, 5	0.741	1, 2, 3	0.57
3B	3,4,5	0.64	1, 2, 3	0.08
NDCI	4,5	0.48	2, 3	0.03
4B/FBS	3,4,5	0.31	1,2,3	0.12

From table 4-5 above, it realised that most of the band combination (NIR-Red-Green band ratios) applied on the simulated data worked well mostly with Landsat-8 simulated data, with MCI and 3B which yielded an R^2 greater than 0.57 having a satisfactory result of an R^2 of 0.74 and 0.64 respectively and NDCI and 4B having performed poorer when testing for their band combination. On the other hand, with SPOT 6 simulated data only the MCI model had a good linear correlation with an R^2 of 0.57. The results showed that Landsat-8 OLI bands were sensitive enough to detect chlorophyll-a concentration than SPOT 6 bands.

4.5. Calibration and Validation

In this research, two types of errors (type I and type II errors) was computed from the calibrated (Cal) and validated (Val) datasets respectively. The absorption coefficient of Chl-a (phytoplankton/pigment) at 440 nm derived from laboratory analysis was divided into calibration and validation datasets and regressed against in-situ reflectance and Landsat-8 and SPOT6 reflectance bands to estimate chlorophyll-a in the selected lakes in this research.
Models calibration was based on the GeoCalVal method by Salama et al., 2012. Eight (8) samples were randomly selected as odd numbers and used to calibrate the algorithm with a linear trend between model chlorophyll-a values and in-situ Chlorophyll-a concentrations (a_pig (440). The remaining eight samples were selected as evens and used to validate the models. Model retrieval or calibration was done using the equation below;

$$a\_chl\ (a_{pig}440)_{cal} = \alpha * (model_{cal}) + \beta \quad \text{..... (Eq. 10)}$$

where $model_{cal}$ can be the calibrated MCI, 3B, NDCI and 4B models and α and β are the slope (beta) and intercept (alpha) derived from the calibrated data set and are constant coefficients that are dependent on a_phy/a_pig (440).
Hence after obtaining these fitting coefficients from the calibrated data sets, we apply that same constants coefficients on the same equation using validated a_phy/a_pig(440) and validated MCI, 3B, NDCI and 4B a_phy/a_pig(440) respectively. This is used to estimate chlorophyll-a (a_phy/pig 440) from the dataset used.

Where α and β were replaced with the coefficients (intercept and slope) derived from the calibrated data set. The resulting values of slope, intercept, R^2, and rMAE were recorded for each model iteration like it was done for the calibration dataset. The error estimators used in this study from gives the probability distributions of the validation errors and were used to test the accuracy of each models.

4.6. Adaptation of Empirical Algorithms used for Estimating Chl-*a*.

A band ratio for each of the models was used to estimate Chl-a from the selected study areas as shown in table 4-3.

4.6.1. New Three-Band (N3B)

The development of the 3 band model by Gitelson was conceptualized by which originally uses three bands at 681, 708, 753 nm) to estimate Chl-*a*. the 3 band model has proven to be robustness to estimate Chl-a in turbid, productive waters (Dall'Olmo & Gitelson, 2006). The 3 band model is based on the relation between the detected reflectance and the total absorption and scattering coefficients respectively (Gitelson et al., 2008). This model, also known as Gitelson model specifically uses three bands at 665, 708, 753 nm rather than the traditional 681, 708, 753 nm in the estimation of Chl-*a* pigments based on inverse reflectance (Rrs^{-1}) and Chl- absorption. The three band model is presented as:

$$(Rrs^{-1}(\lambda_1) - (Rrs^{-1}(\lambda_2)] * Rrs(\lambda_3) \quad \text{..... (Eq. 12)}$$

Where $Rrs^{-1}(\lambda_1)$, ($Rrs^{-1}(\lambda_2)$, are the inverse of remote sensing reflectance at wavelength 1, 2 and Rrs (λ_3) is the remote sensing reflectance at wavelength 3. The wavelength (λ_1), (λ_2) and (λ_3) are the wavelengths of the three bands in increasing order.
From equation 12, Chl-*a* is stated as function of inverse Rrs. $Rrs^{-1}(\lambda_1)$ which belong to 660 nm- 690 nm band width and this band (λ_1) must be strongly sensitive to absorption of phytoplankton/pigment while $Rrs^{-1}(\lambda_2)$ is least sensitive to Chl-*a* absorption found between 710 – 730 nm band width (Dall'Olmo & Gitelson, 2006). In order to eliminate the influences of CDOM and TSS as well as NAP, the second band, that is ($Rrs^{-1}(\lambda_2)$) is must be subtracted from $Rrs^{-1}(\lambda_1)$. Mostly Rrs (λ_3) is introduced to reduce the influence of any backscattering and must be practically less affected by water constituents such as CDOM, NAP and SPM.

The Rrs (λ_3) is used in this case because it is assumed that absorption and backscattering is non-negligible. Hence absorption at λ_3 can be solely attributed to the influence of pure water (Dall'Olmo & Gitelson, 2006).

4.6.2. The Maximum Chlorophyll Index (MCI)

This model was originally developed by (Gower et al., 2005; Gower et al., 2008) for MERIS sensor processing scheme and is used to investigate the seasonal dynamic, spatial distribution and coverage of blooms. The development of the MCI model was based on the concept of the Florescence Line Height (FLH) designed for MODIS sensor.

Likewise the FLH algorithm, the Maximum Chlorophyll Index (MCI) algorithm is a measure of reflectance height or total water leaving radiance at 709 nm which is notably referenced against linear baseline of two neighbouring wavelengths of either 681 or 753 nm respectively. The MCI band model is presented as:

$$(Rrs\lambda_1) - (Rrs\lambda_2) * \frac{(\lambda_2 - \lambda_1)}{(\lambda_2 - \lambda_1)} * (Rrs\lambda_3) - (Rrs\lambda_1)$$

This model use bands centered at 665, 708, 753, all of which belong to the red and the infrared (NIR) spectral bands respectively (Gower et al., 2008). The spectral response band above a linear baseline between a wavelengths of 681 and 753 (in some other cases 665, 753) indicates a high surface concentration of chlorophyll-*a* against a scattering background which means they are least affected by CDOM and TSM (Gower et al., 2005; Gower et al., 2008 and Blondeau-Patissier et al., 2014). Although detection of Chl-*a* using MCI might be unique to only the MERIS sensor, it could also be estimated with the use of other existing or new Multi-spectral sensors and it is therefore widely applicable to different remote sensing systems (Alikas et al., 2010).

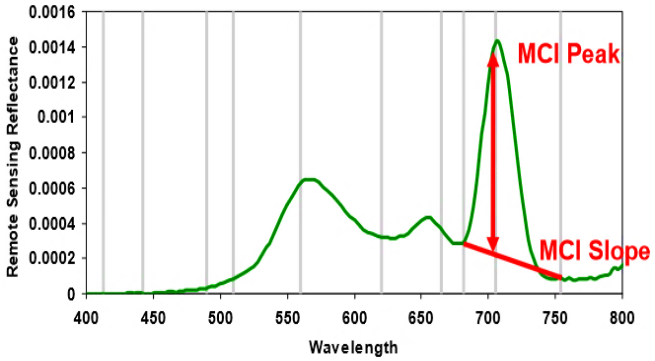

Figure 4-4: Schematic representation of the MCI model/algorithm.

4.6.3. Normalized Difference Chlorophyll Index (NDCI)

The Normalized Difference Chlorophyll Index (NDCI) algorithm was developed by (Mishra & Mishra, 2012) based on the concept of Normalized Difference Vegetation Index (NDVI) to predict Chl-*a* concentration from satellite images. This is because of the complexity of the use of the NDVI model in estimating Chl-*a* in water bodies. This led to the development of the NDCI model as defined in equation 9, makes it easier in the estimation of Chl-a. This model is a straight forward one that uses bands at 665 nm - Rrs (665) and 708 nm - Rrs (708) and makes it possible for binding higher and lower index values ranging between -1 and 1. The NDCI band model is presented as:

$$C_{chla} = \frac{[(Rrs\ (\lambda_2) - (Rrs(\lambda_1)]}{[(Rrs\ (\lambda_2) + (Rrs(\lambda_1)]} \quad \text{..... (Eq. 13)}$$

Where Rrs (λ_1) and Rrs (λ_2), are remote sensing reflectance at wavelength 1 and 2 in the NIR and Red bands respectively. Likewise other algorithms, this model uses information based on the reflectance peak at 708 nm which is maximally sensitive to differences in Chl-a concentrations in water. The bands at 665 and 708 are normally used to eliminate the influences of other water leaving constituents such as CDOM, and NAP. The NDCI model was developed to take the spectral difference in the bands at 708 nm (NIR band) and 665 nm (Red band) and normalizing it by the sum of their reflectance to eliminate influences and uncertainties (Mishra & Mishra, 2012).

4.6.4. Four Band (TBS)

Based on improving accuracy and performance of the 3 Band model, the four band algorithm was developed by (Le et al., 2009). The four band model was derived from equation 8 of the three band model in section 4.4.2 by replacing the only Rrs (λ_3) found in the three band model with $[Rrs^{-1}\ (\lambda_4) - Rrs^{-1}\ (\lambda_3)]^{-1}$. Hence it takes the following form;

$$[(Rrs^{-1}(\lambda_1) - (Rrs^{-1}(\lambda_2)] \times [(Rrs^{-1}(\lambda_4) - (Rrs^{-1}(\lambda_3)]^{-1} \quad \text{..... (Eq. 14)}$$

The introduction of Rrs (λ_4) in the four band model in equation 14 removes or minimizes the effects of high absorption of suspended particles and backscattering of over the R-NIR region.

The similarities between these models or algorithms used could be that they all use similar spectral bands that normally is used to eliminate the effects and influences of water leaving constituents such as NAP, CDOM and TSM and among others. Differences in

4.7. Algorithm Evaluation and Assessment

The accuracy of each model used was assessed using the validated datasets between estimated and ground truth values. Standard statistics were used to assess the accuracy of the models discussed in section 4.4. The performance of each algorithm was weigh based on statistic metrics used in equations 8-10 including rMAE –(Relative Mean Average Error-Equation 10), and R^2 (coefficient of determination).

$$MAE=\frac{1}{n}\sum_{i=1}^{n}(x_{1-}x_2) \quad \text{..... (Eq. 15)}$$

$$rMAE=\frac{1}{n}\sum_{i=1}^{n}\left(\frac{(x_1-x_2)}{x_i}\right) \quad \text{.....(Eq. 17);}$$

where **n** is the number of observations/samples, $\mathbf{x_1}$ is the Chl-a values actually observed from Landsat-8 or SPOT6 and $\mathbf{x_2}$ is the Chl-a values estimated from the field. However, these statistic metrics values will be used to distinguish model performance as well as to compare the individual model performance.

4.8. Software packages

Three software packages were used in this study. They include ENVI version 5.3 which was used for atmospheric correction, spectral resampling and band-math to create chlorophyll-a concentration maps. The Matlab software was also used to write codes for shaping model/algorithm application and producing probability distribution of least squares and lastly ArcGIS version 10.1 software was used to process, analyse and sharpen and chlorophyll-a images.

5 RESULTS

5.1. Water Constituent Concentrations from the field

Most European lakes bear the characteristics of a case 2 water which is not only affected by phytoplankton but by other water constituents such as CDOM, non-algal pigments (NAP), and total suspended materials (TSM). After analysis at the laboratory, many concentrations of water constituent were observed and they vary from one lake to another lake. The lakes studied indicates a typical case 2 lakes. This is more discussed in section 5.2 below.

5.1.2. Relationship between Chl-*a* Concentration and Absorption Coefficient of CDOM at 440 nm.

The data showed a wide range of constituent composition and varying optical properties. To determine whether the lakes are case 1 or case 2 water, a simple regression was analyzed for the lakes. The coefficient of determination (R^2) for the linear relationship between Chl-*a* and CDOM shown in figure 5-1 was poor and lower than 0.1 m^{-1}.

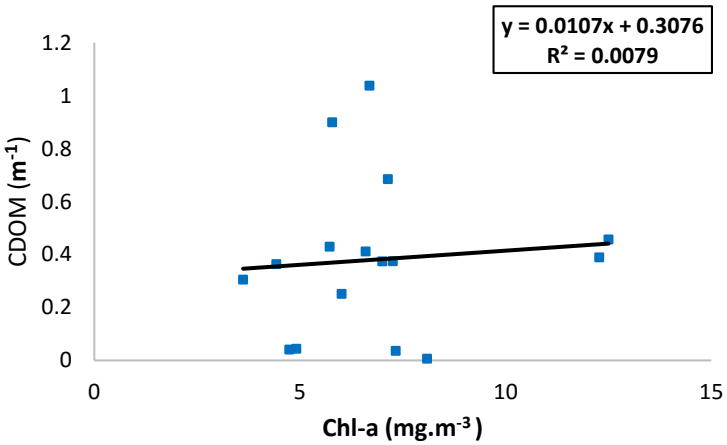

Figure 5-1: Correlation between CDOM and Chl-a concentration.

From figure 5-1, it can be seen that the lack of a significant relationship between Chl-a and CDOM indicates that the lakes (waters) was independently controlling optical properties of the lakes. Chl-a and CDOM were not correlated. This rightly confirms that the lakes in question are all case-2 waters (Morel & Prieur, 1977). Concentrations of Chl-*a,* absorption coefficient of Chl-a (phytoplankton pigments at bands 440 nm and 665 nm), absorption coefficient of CDOM also at 440 nm were measured at the laboratory from collected water samples from each of the sites. Chl-a concentrations for Lake Binnenschelde, Markiezaatsmeer and Hulsbeek varies from 3.81 $mg.m^{-3}$ to 23.7 $mg.m^{-3}$. The trophic state of each of the lakes were determined based on the Chl-a measurements (results) from the laboratory (Thiemann & Kaufmann, 2000). The concentrations level Chl-a in Lake Binnenschelde, Markiezaatsmeer and Hulsbeek indicates that the lakes are eutrophic in nature (Megard et al., 1980).

However, for Lake Binnenschelde, Markiezaatsmeer, and Hulsbeek, there were significant analyses of water quality variables mentioned above. The lowest absorption coefficients CDOM were recorded in Lake Hulsbeek with a value of 0.005 m^{-1} and the maximum absorption coefficients CDOM recorded in Lake Binnenschelde of a value of 0.30 m^{-1}. Hence, the overall absorption coefficient of CDOM for these study sites were very low. This may be due the less presence of sediments and phytoplankton observed in the lakes. From the results provided in table 5-2, it can noted that Chl-*a* measurements were generally lowest in Lake Binnenschelde giving an indication that Lake Binnenschelde is the clearest lake was with mean of 5.22 mg/m^{-3} and a standard deviation of 0.29 mg/m^{-3} with Lake Markiezaatsmeer recording the highest Chl-a concentration (a minimum of 6.01 mg/ m^{-3} and maximum of 12.5 mg/m^{-3}) among the lakes used for this study. The absorption of phytoplankton at band 440 nm ranges from 0.06 m^{-1} to 0.20 m^{-1} for Lake Binnenschelde, 0.04 m^{-1} – 0.22 m^{-1} for Lake Binnenschelde and 0.30 m^{-1} to 0.68 m^{-1} for Lake Hulsbeek respectively.

The minimum, maximum, mean and standard deviation of measured Chl-a (mg/ m^{-3}), absorption of CDOM and absorption of Chl-a (m^{-1}) at band 440 and 665 nm for the five (5) lakes is presented in table 5-1 below.

Table 5-1: Statistical summary of water constituent concentrations for Lakes Markiezaatsmeer, Binnenschelde and Hulsbeek.

Basin	n	Constituents	Statistical Description			
			Min	Max	Mean	SD
Markiezaatsmeer	6	Chl-*a* (mg/m^{-3})	6.01	12.50	8.60	2.95
		a_{CDOM} (440)(m^{-1})	0.250	0.456	0.375	0.686
		a_{ph} (440)(m^{-1})	0.108	0.198	0.163	0.029
		a_{ph} (665)(m^{-1})	0.065	0.101	0.089	0.013
Binnenschelde	4	Chl-*a* (mg/m^{-3})	3.62	7.14	5.22	1.54
		a_{CDOM} (440)(m^{-1})	0.304	0.684	0.445	0.167
		a_{ph} (440)(m^{-1})	0.132	0.297	0.193	0.072
		a_{ph} (665)(m^{-1})	0.080	0.168	0.110	0.039
Hulsbeek	6	Chl-*a* (mg/m^{-3})	4.74	8.09	6.25	1.34
		a_{CDOM} (440)(m^{-1})	0.005	1.03	0.34	0.48
		a_{ph} (440)(m^{-1})	0.323	0.559	0.427	0.097
		a_{ph} (665)(m^{-1})	0.153	0.264	0.202	0.043

5.1.3. Spectral Analysis for remote sensing reflectance and Absorption Coefficient of Chlorophyll-*a*

The chlorophyll-a (phytoplankton pigment) absorption coefficient from laboratory measurement and the remote sensing reflectance were analyzed for Lakes Binnenschelde, Markiezaatsmeer and Hulsbeek. The retrieval were between the wavelength range of 300 nm and 900 nm. The wavelength range based on the limitation to the spectra ranges for this study. The relationship between the spectral responses and measured absorption of Chl-*a* pigments was determined based on the algorithms or models that was used in this study. This is to say that a model that proved a very strong relationship between index values derived from each algorithm against measured absorption coefficient of phytoplankton/pigment was used to generally map Chl-*a* concentration (absorption coefficient of phytoplankton) for each lakes. The minimum and maximum of the absorption spectra of phytoplankton/pigment is presented in table 5-2.

5.2. Summary of Reflectance and absorption Spectra Characteristics from the study sites

Basically, turbid water(s) were observed during the three (3) field campaigns for Lakes Markiezaatsmeer, Binnenschelde and Hulsbeek. According to the RAMSES radiometric data of Lake Markiezaatsmeer, Binnenschelde and Hulsbeek on 23rd, 24th and 26th September, 2015, the wavelength ranges from 300 nm to about 1000. But based on the limitation of spectral bands used for this research, only band width ranging from 400nm to 900nm were used. Reflectance spectra in Figure 5-2 (a- c) shows two relatively low peaks at 440 nm and 650 which belong to the blue and the red regions respectively. The relatively low peaks at 440 nm and around 650 were used in the retrieval of Chlorophyll-*a* against field observed Chlorophyll-*a* concentration. Remote sensing reflectance of each of the lake varies greatly over the visible and NIR spectral regions. These were all radiance and reflectance values obtained from above water measurements using RAMSES (ACC and ARC) -Trios sensors for Markiezaatsmeer, Binnenschelde and Hulsbeek respectively. The spectral characteristics of these four (4) lakes were similar in shape and their magnitude and peaks mostly ranging between 550 nm – 750 nm. The spectral reflectance curves of each lake is shown in figure 5-2. Again, the minimum, maximum, mean and standard deviation of measured Spectral Remote Sensing Reflectance observed from the field

Table 5-2: Summary statistics Spectral Remote Sensing Reflectance Values Observed in each study area. (sr^{-1}).

Basin	Date Obtained	n*	Min	Max	Average	Median	St. Dev.
Markiezaatsmeer	23 - 09 – 2015	20	0.0014	0.0509	0.0103	0.0091	0.0054
Binnenschelde	24 - 09 - 2015	15	0.0086	0.0325	0.0101	0.0084	0.0051
Hulsbeek	26 - 09 - 2015	10	0.0027	0.0171	0.0100	0.0103	0.0015

5.2.1. Reflectance and absorption Spectra Behaviour of selected Lakes Lake Markiezaatsmeer, Binnenschelde and Hulsbeek.

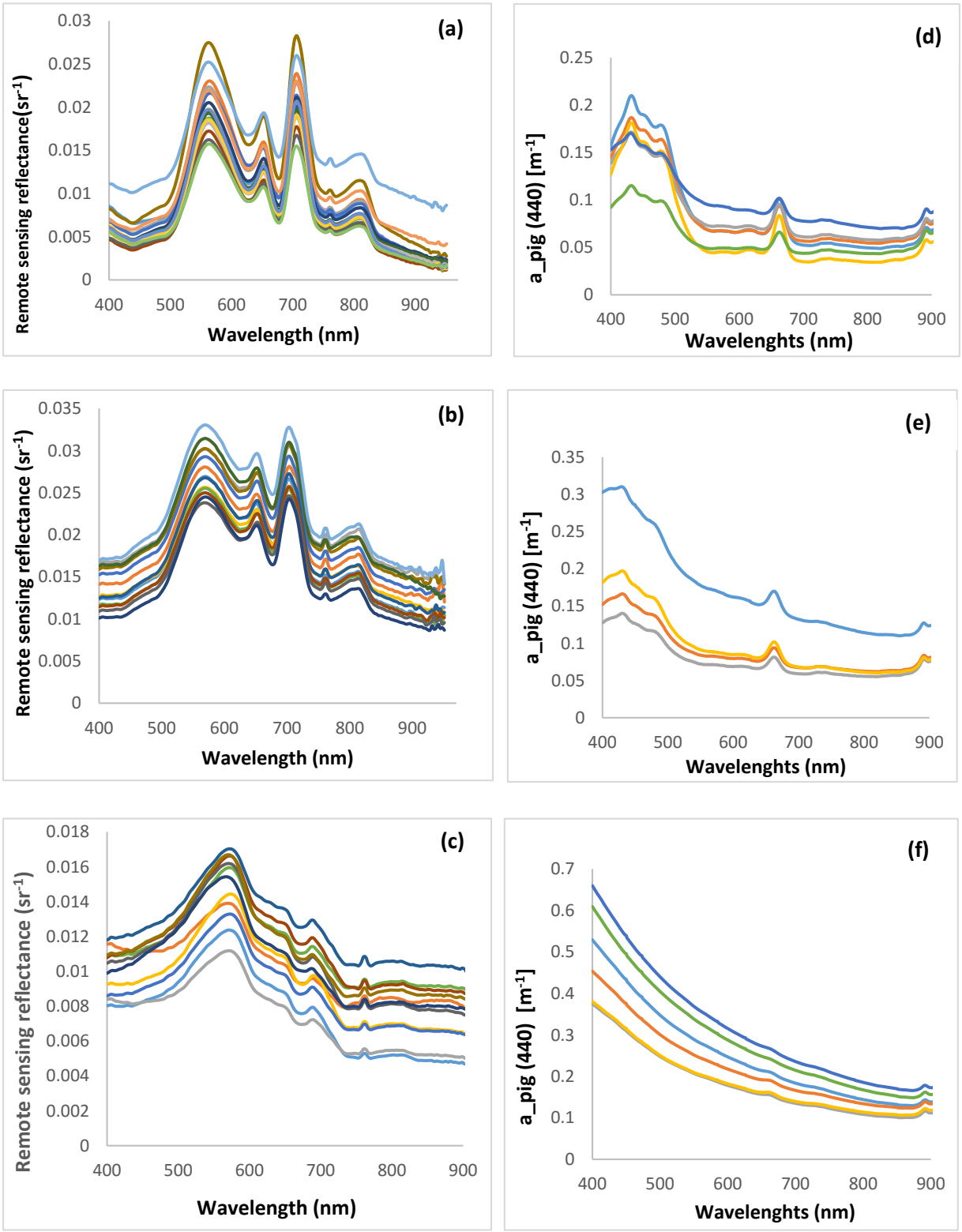

Figure 5-2: TRIOS-RAMSES-Reflectance Spectra (Rrs) observed in (a) Markiezaatsmeer, (b) Binnenschelde and (c) Hulsbeek; and Laboratory measured absorption coefficient of phytoplankton/pigments for (d) Markiezaatsmeer, (e) Binnenschelde and (f) Hulsbeek.

The wavelengths between 300 and 900 nm was selected for analysis for both radiometric data. The reflectance spectra of samples form the four (4) field campaigns are shown in figure 5-2 (a-c) and these field spectra are similar in shape and magnitude and also similar to that of typical productive turbid water (Gitelson et al, 2007). From figure 5-2 (a-c), it can be noticed that there is a significant reflectance peak around the green range 500 -570 nm which decreases gradually and it is attributed to phytoplankton spectral behaviour. Subsequently, there is another trough near 685 and around 700 nm for figure 5-2 (a & b) demonstrating the dominance of both backscattering of Chlorophyll-a and minimal absorption of accountable water constituents including pure water in the three (3) lakes except for Lake Hulsbeek, hence there is maximum chlorophyll-a is located in the red band (Gurlin et al, 2011). It can also be noticed that there is a remarkably low reflectance in the blue region around (400-500) nm due increase in Chlorophyll-a pigment. This is due to an increase absorption of Chlorophyll-*a* pigment, NAP, and CDOM (Gitelson et al, 2009). Theses reflectance spectra shows a low reflection and high absorption levels when wavelength is greater than 750 (700-750 nm) nm in the NIR region, comparably with that of the blue region (400-500 nm) and this is an attribute of all typical turbid water especially lakes. In this NIR region in particular, reflectance is mostly controlled by scattering of particulate matter. However, increases in the water-leaving reflectance have been associated with the increase in backscattering, hence increase in absorption increases decreases the water leaving reflectance in a every part of the spectrum (Morel & Prieur, 1977). Another peak reflectance is observed around 810 nm attributed also to organic matter constituents and chlorophyll (Rundquist et al, 1996). Hence the variation in the level of the spectral curves observed in the study area of this research is due to the absorption and scattering of the presence of suspended, particulate and dissolved matter. On the other hand, the absorption of phytoplankton/pigments at 440 nm and 665 nm and CDOM at 440 nm, together with matter components have great spatial difference.

On the other hand, the absorption spectra due to phytoplankton/pigments in figure 5-2 (d –f) have two distinctive features; one is the absorption spectra location at near 440 nm in the blue spectral region and the other near 670 nm (Ma et al, 2006). The in-situ absorption of chlorophyll-a pigments/phytoplankton from the three lakes (Binnenschelde and Markiezaatsmeer) showed a wide variation in the red spectral absorption coefficient around 665 nm. However, Lake Hulsbeek showed a different variation in the red spectrum. This may be due to package effect and variation in pigment composition of phytoplankton cells and physiological feature of the lakes, including temperature, light availability and nutrients (Bricaud et al, 1995). The absorption coefficients of Chlorophyll-a pigments with peak around 440 nm varied from 0.108 to 0.198 m^{-1} while the absorption coefficients of Chlorophyll-a pigments with peak around 665 nm varied from 0.065 to 0.101 m^{-1} for Lake Markiezaatsmeer. With Lake Binnenschelde and Hulsbeek, the absorption coefficients of Chlorophyll-a pigments with peak around 440 nm varied from 0.132 to 0.297 m^{-1} and 0.323 to 0.559 m^{-1} while near 665 nm 0.080 to 0.168 m^{-1} and 0.153 to 0.264 m^{-1}respectively.

5.3. Accuracy of Atmospheric Correction Method

After the application of the FLAASH atmospheric correction method on both landsat-8 and SPOT-6 images, few observations were made. The remote sensing reflectance (Rrs) values for the Landsat-8 images and concurrent in-situ showed a good correlation than compared to SPOT-6. Comparing the averaged reflectance of the atmospherically corrected Landsat-8 image and in-situ reflectance measurements for Lake Markiezaatsmeer and Binnenschelde 27th September, 2015 showed a robust consistency and a good correlation. On the other hand, there was a good match between atmospherically corrected image Rrs and in-situ Rrs for Lake Hulsbeek on the 29th September, 2015. However, atmospheric correction (FLAASH) provided poorer results application on SPOT- 6 images, hence it was not displayed in my results. The results of SPOT 6 did not show much correlation against in-situ reflectance hence the results from SPOT6 atmospheric correction was not presented. There were some poorer results from the atmospheric correction which were not displayed. This could be attributed to residual adjacency effects or wrong aerosol model parameterization which causes low reflectance in the NIR spectrum (Guanter et al., 2010). The accuracy of the results from this study is shown in figure 5-3 and these results follows similar results observed by (Collin & Hench, 2012; Guanter et al., 2010 and Song et al., 2012). Table 5-3 below shows the R^2 and RMSE of two selected study areas from each image.

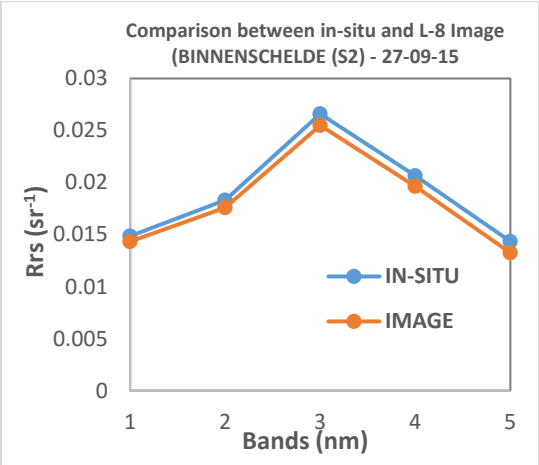

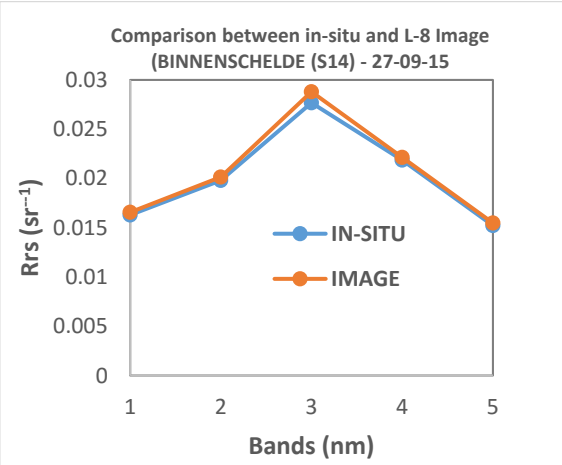

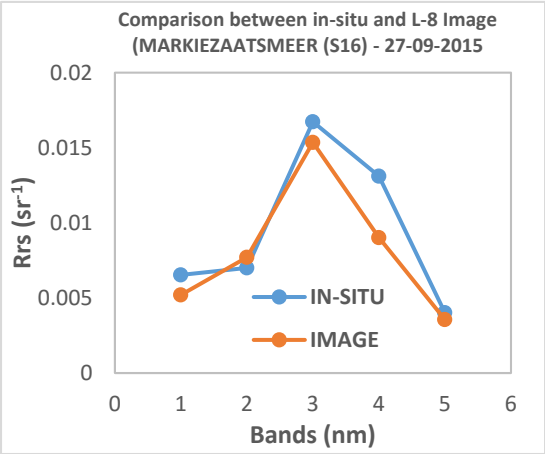

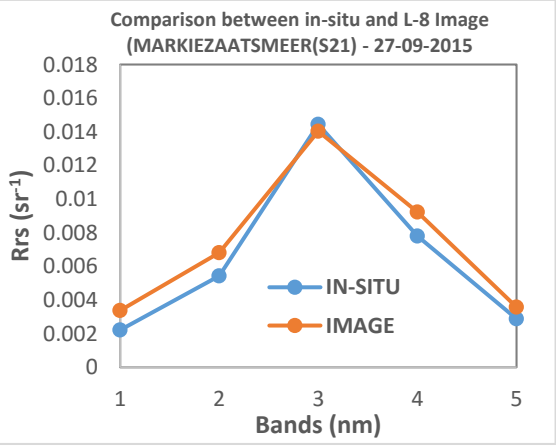

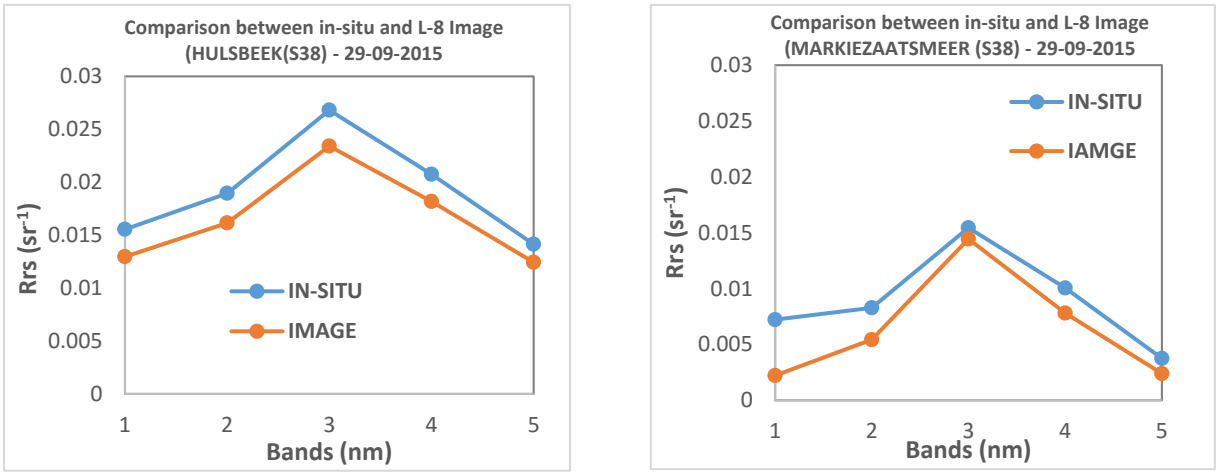

Figure 5-3: Comparison between in-situ reflectance and Landsat-8 reflectance spectra.

Six samples, which include two samples for each lake were collected few days after the landsat-8 overpass on 27th and 29th September, 2015 for all lakes. These were used to evaluate the performance of the atmospheric correction as shown in figure 5-3. Only the best results of the outcome of the atmospheric correction method was showed. This is comparing in-situ remote sensing reflectance with Landsa-8 reflectance spectra at selected sites, two for each study are respectively. Details of the results of the atmospheric correction is presented in table 4-4.

Table 5-3: Results of the atmospheric correction method compared with in-situ reflectance for selected sites (at least two sample points) from each of the three study areas.

Study Site	Image Date		R2	RMSE
Lake Binnenschelde	27th September, 2015	S2	0.998	0.000560
		S14	0.997	0.000918
Lake Markiezaatsmeer	27th September, 2015	S16	0.911	0.002866
		S21	0.892	0.002056
Lake Hulsbeek	29th September, 2015	S38	0.985	0.00108
		S43	0.955	0.002668

5.4. Calibration and Validatiion of all Data Sets.

In this study, all the calibration and validation values (in-situ a_chl and in-situ and simulated Rrs) from datasets were chosen based on a fair selection. Radiometric and laboratory datasets measure were divided into two: one for calibration as calibration dataset and one for validation as validation datasets. The GeoCalVal method was used as discussed in section 4.4. Most of the algorithms adapted from table 4-3

worked well with both in-situ and satellite data when plotted against the in-situ absorption coefficients of phytoplankton/pigments. Only algorithms that uses mostly three (3) bands and four (4) band were tested on field data, and Landsat-8 bands as well as SPOT6 bands. The structure proposed for best fitting of an empirical model for retrieving Chl-a in this study are presented in equation 13/14;

$a_{pig(440)} = \alpha * (\text{Model}) + \beta$ …… (Eq. 14)

Where: α and β are the fitting coefficients and a_{pig} (440) is the absorption coefficient of chlorophyll-a pigment at 440 nm.

The MCI, 3B, NDCI and 4B algorithms were tested to use both bands of maximum and minimum reflectance and absorption and wavelength band ranges respectively. Simply put, both single band values and band maximum and minimum reflectance and absorption were used to set the accuracy of each model. In all, after executing this exercise, single band ratio seem to perform better than band maximum and minimum reflectance based on the data from the study areas of this research. From this a regression plots (on probability curves) were performed in Matlab software to determine the fitting coefficients for the estimation or prediction of Chl-a absorption for the three (3) lakes under study. The MCI, 3B, NDCI and 4B models were then weighted using these statistical indexes: R^2 and rMAE.

5.5. Calibration of In-Situ Data Sets

In previous studies, single band, band ratio and one order derivatives methods were used to estimate Chl-a or chlorophyll-a absorption coefficient. However, in this study, more than two bands or at least 3 band reflectance models were used to estimate Chl-a(absorption coefficients of Chl-a) in this study. These models were tested and their accuracy and performance were assessed concurrently with both field in-situ data and satellite data (Landsat-8 and SPOT6). Model calibration was done with half of the dataset that is 8 sample points out of 16 sample points used in this study. The MCI, 3B, NDCI, 4B and SCI algorithms were calibrated using the type I statistical least square regression method. All the models were calibrated using a linear function as in equation 14; Chl-a = α (*model*) + β, where α and β are fitting coefficients derived from calibrated data and *model* could be MCI, 3B, NDCI, 4B and SCI. Table 5-4 shows the coefficients obtained from calibrating in-situ chlorophyll-a absorption with in-situ model reflectance. This result are similar results by other researchers (Mishra & Mishra, 2012; Gurlin, Gitelson, & Moses, 2011).

Table 5-4: Coefficients derived from model calibration applied to field data.

Model	Model Calibration (Cal set) Summary	
	Slope (α)	Intercept (β)
MCI	-12.755	0.257
3B	-0.436	0.214
NDCI	-0.491	0.211
FBS	-0.495	0.238

From table 5-4 shows the results of the calibration analysis. It is clear that only positive of intercept was found for the MCI, 3B, NDCI and 4B/FBS. A positive value of intercept could means that at a given concentration, a model might have no response to spectral signatures. But this is not a typical response of a Chl-a model (Augusto-Silva et al., 2014). See appendix for calibration results plotted with Matlab software.

5.6. Validation of In-Situ Data Sets

Validation of calibrated algorithms or models were done for the rest of the data sets using the linear best fitting coefficients α and β to derive from table 5-4. The performance of the four algorithms that was used to derived Chl-a concentration from in-situ data was tested by validating ground measured Chl-a and TRIOS-RAMSES (in-situ) reflectance. Regression plots of algorithm index reflectance values were plotted against absorption coefficient of phytoplankton (a_chl-*a*) for the various study sites. In totality, the algorithms or models were evaluated using the statistical metrics presented in equation 8, 9 and 10 in sub-section 4.4. The coefficients of determination (R^2) and the percentage error (rMAE) were calculated for each of the model respectively. The statistical summary of the results of validation of models from field (in-situ) data is presented in table 5-5 and figure 5-5 below. The model parameters were estimated from the calibration datasets.

Table 5-5: Summary results of model validation process (model performance) for in-situ data.

Model	Model Validation/Performance on (Val set) for TRIOS RAMSES			
	Slope	Intercept	R^2	rMAE (%) (m^{-1})
MCI	0.922	0.013	0.69	18.34
3B	0.867	0.021	0.54	23.30
NDCI	0.952	0.006	0.45	21.33
FBS	***0.935***	***0.010***	***0.83***	***12.35***

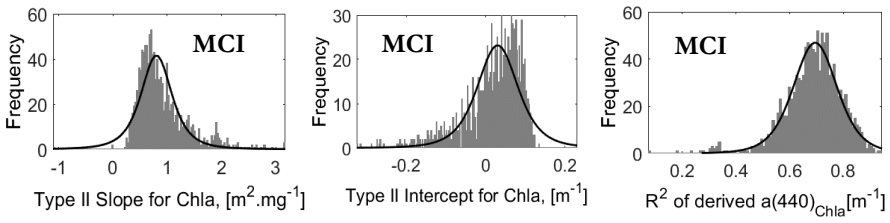

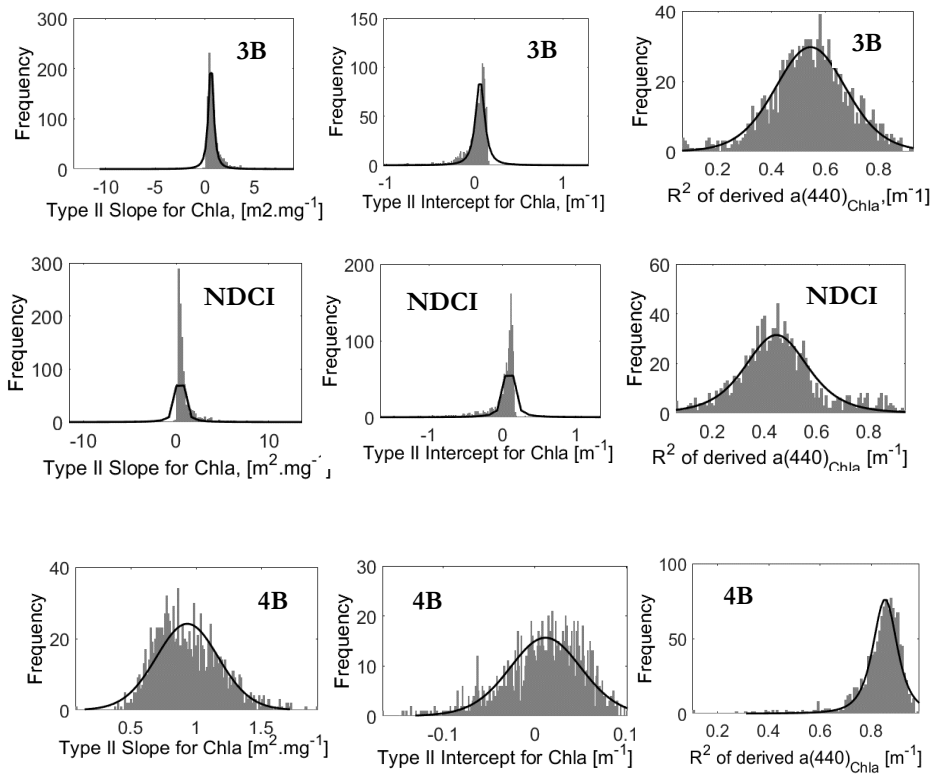

Figure 5-4: Probability distribution of validation process for MCI, 3B, NDCI and 4B models or algorithms using field data.

Figure 5-4 which contains four scatter diagrams each for each model shows the results of Chl-a estimation using MCI, 3B, NDCI and 4B

From table 5-5 and figure 5-5, it is observed that the 4B and MCI models performed well when applied on in-situ data. These models that come close to the 1:1 line. The relationship between the 4B and MCI estimated absorption of Chl-a and measured absorption of Chl-a were linear functions and had a strong relationship with R^2 of 0.83 and 0.69 respectively (see table 5.5 & figure 5-6 a& d).

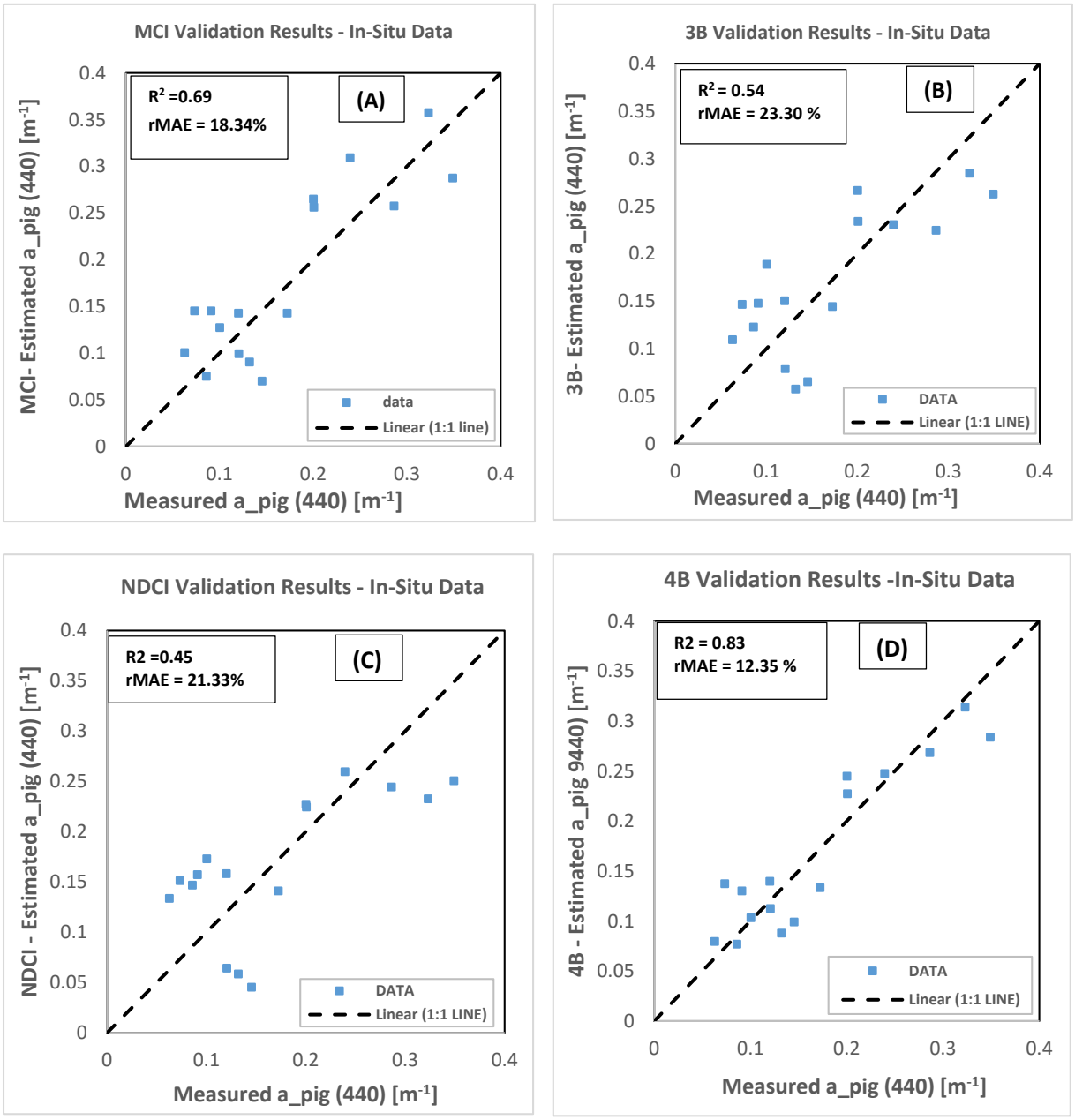

Figure 5-5: Scatterplots of the measured versus estimated a_pig (440 nm) using field data for the various models.

5.7. Calibration of Simulated Landat-8 OLI And SPOT6 Data Sets

The same methodology applied on the derivation of chlorophyll-a (a_pig (440)) from in-situ data was applied on both Landsat-8 OLI and SPOT data sets respectively. With these simulated bands, the same calibration and validation process was repeated both for landsat-8 and SPOT6. Table 5-6 and 5-7 shows the calibration results for Landsat-8 and SPOT6 simulated bands. After analysis and application of the model, it was realised that the models worked well with Landsat data likewise in-situ data and they both had a similar pattern of results with MCI, 3B, NDCI and FBS having negative slopes. The only model that had a negative intercept was SCI model. On the other hand, four out of the five models could not work well when applied to SPOT6

data apart from the MCI model. However, only the MCI model worked well with SPOT 6 after its application. Hence, it is clearly noted that model application worked well with Landsat-8 data more than SPOT6 as seen in tables 5-6 and 5-7.

Table 5-6: Coefficients derived from model calibration applied to Landsat-8 datasets.

Model	Model Calibration (Cal set) for Landsat-8	
	Slope	Intercept
MCI	-0.037	0.011
3B	-2.002	0.533
NDCI	-1.434	0.397
FBS	-2.838	1.308

Table 5-7: Coefficients derived from model calibration applied to SPOT6 datasets.

Model	Model Calibration (Cal set) for SPOT6	
	Slope	Intercept
MCI	2.413	-0.234

5.8. Validation of Simulated Landat-8 OLI and Spot6 Data Sets

The equations in table 5-6 were validated for Landsat- 8 and the MCI model had the best validation performance with R2 of 0.753 and rMAE of 0.06 m^{-1} and 21.29% (table 5-7). This value is higher than the value found from the best validation performing model (FBS/4B) model using in-situ data of R2 of 0.753, and rMAE of 0.035 m^{-1} and 12.35%. The results for best performing model for in-situ data is lower could be associated with differences to band response (Augusto-Silva et al., 2014). This is to say that the positions of Chl-*a* features may shift and this could or may affect the results from both in-situ and Landsat- 8 dataset. When models were compared for both in-situ and Landsat-8 data, the NDCI model proposed by (Mishra & Mishra, 2012)seem to the worst performing model which did not have a good linear relationship with measured Chl-a. The NDCI model had the lowest performance when compared with other tested models (Watanabe et al., 2015).

Table 5-8: Summary results of model validation process (model performance) for Landsat-8 dataset.

Model	Model Validation/Performance on (Val set) for Landsat-8			
	Slope	Intercept	R^2	rMAE (%)
MCI	***1.388***	***-0.055***	***0.75***	***21.29***
3B	1.408	-0.068	0.65	24.21
NDCI	1.916	-0.147	0.50	32.68
FBS	4.151	-0.544	0.37	59.64

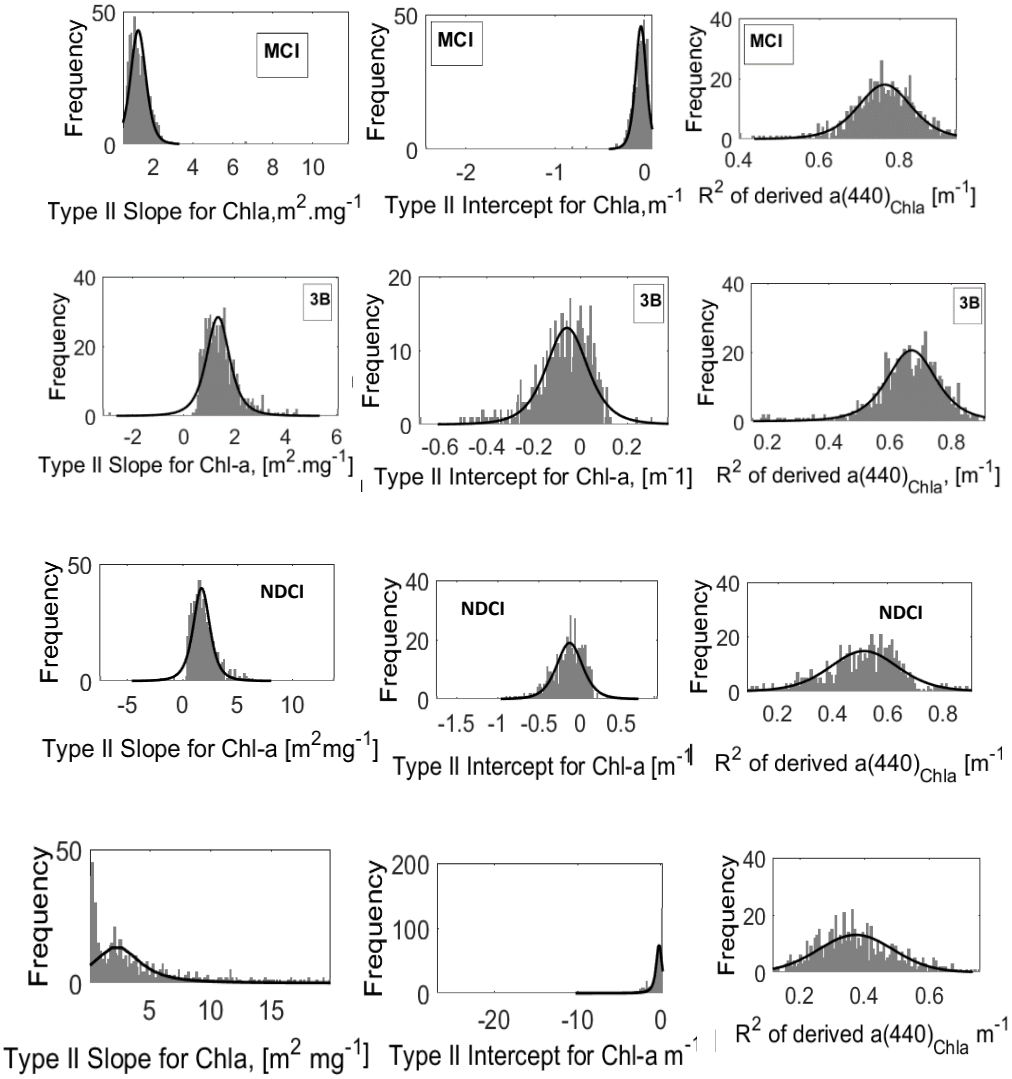

Figure 5-6: Probability distribution of validation process for MCI, 3B, NDCI, and 4B models using simulated Landsat-8 data.

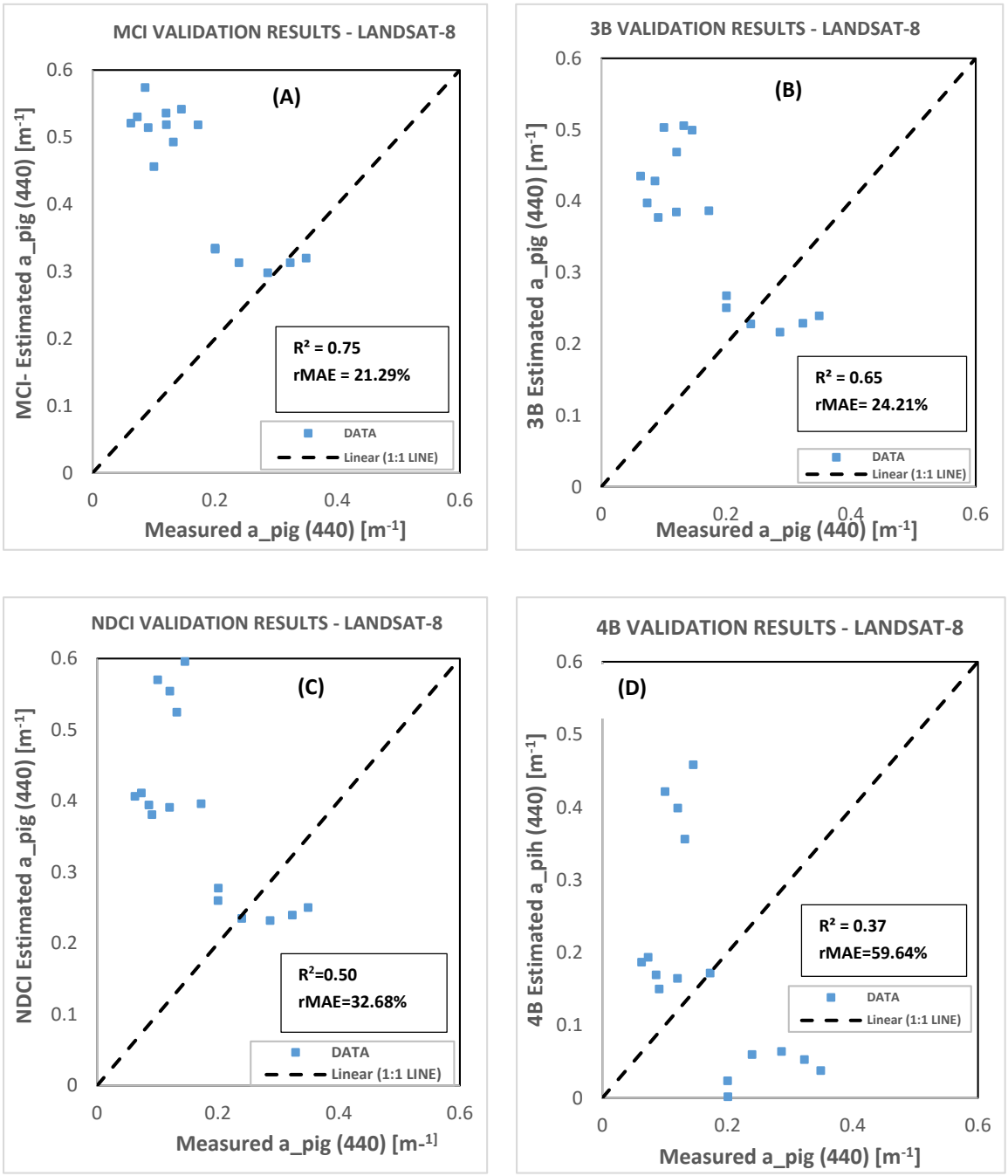

Figure 5-7: Scatterplots of the measured versus estimated a_pig (440 nm) using Landsat-8 data for the various models.

In the application of the models on Landsat-8 data set generated greater error as compared to spot-6. The rMAE increased when model was applied to the simulated Landsat-8 dataset. This denotes that applying the same algorithm on different dataset can cause a growth in error of estimating Chl-a. Beside the growth of error, the MCI proved to work well with Landsat-8 data and had a better performance ahead of 3B, NDCI and 4B. The scatterplot in figure 5-8 shows that all algorithms diverged from the 1:1 line, that's why error became greater as compared to results from in-situ data. Hence, the MCI model proved to be more

compatible with Landsat-8 data likewise SPOT6 as shown in figure 5-9. However, despite the difficulties in tuning the MCI to estimate Chl-a from the various datasets used, the Maximum Chlorophyll Index with R^2 from the filed data, Landsat-8 data and SPOT6 data to be 0.69, 0.75 and 0.43 and rMAE to be 18.34%,21.29% and 41.25% respectively emerged as the best algorithm based on performance.

Table 5-9: Summary results of model validation process (model performance) for SPOT6 data.

	Model Validation/Performance on (Val set) for SPOT6			
Model	**Slope**	**Intercept**	**R^2**	**rMAE (%)**
MCI	***2.413***	***-0.234***	***0.58***	***41.258***

The 3B, NDCI, 4B and SCI models were not validated for SPOT 6 data due to the poor performance. Hence only MCI model showed a strong linear relationship. However, the results of only MCI was shown for analysis because other four models including, 3B, NDCI, 4B and SCI could not estimate absorption of chlorophyll0a pigments in all form the data set used. Although the linear relationship for MCI model was not that strong when directly applied on SPOT 6 data set, it can be seen that it worked with concurrent dataset for TRIOS RAMSES, Landsat-8 and SPOT6, henceforth the Maximum Chlorophyll Index was chosen to be the best model that can be used to quantify or estimate Chl-a in inland waters based on the study areas selected for this study.

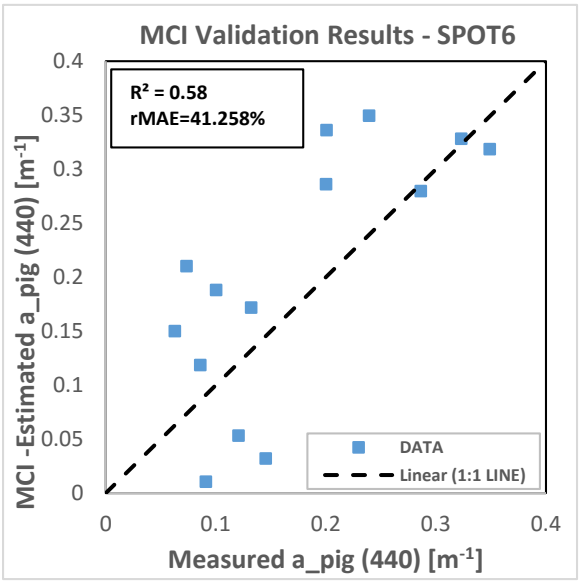

Figure 5-8: Scatterplots of the measured versus estimated a_pig (440 nm) using SCI data for only the MCI model.

6. DISCUSSION

This chapter expatiates the research questions and discusses the outcome of the methodology implemented in achieving the research questions and the objective of this study.

In most cases, especially for the analysis of reflectance spectra in turbid productive water, as discussed in section 5.1.1., an increase in the water-leaving reflectance have been mostly associated with the increase in backscattering due to the absorption and scattering of the presence of suspended, particulate and dissolved matter. This lead to an increase in absorption thus decreases the water leaving reflectance in every part of the spectrum. (Morel & Prieur, 1977).

Normally, the absorption spectra due to phytoplankton pigments have two distinctive features; one is the absorption spectra location at near 440 nm in the blue spectral region and the other near 670 nm (Ma et al, 2006). The materialized in-situ absorption of chlorophyll-a pigments/phytoplankton from the three lakes (Binnenschelde, Markiezaatsmeer and Hulsbeek) showed a wide variation in the red spectral absorption coefficient around 440 nm. However, Lake Hulsbeek showed a different variation in the red spectrum and it should be noted that an absorption spectra at a peak near 665 nm is also predictable. The differences of absorption of phytoplankton/pigments in most part of the wavelength spectrum may be due to package effect and variation in pigment composition of phytoplankton cells and physiological feature of the lakes, including temperature, light availability and nutrients (Bricaud et al, 1995). The absorption coefficients of Chlorophyll-a pigments with peak around 440 nm varied from 0.108 to 0.198 m^{-1} while the absorption coefficients of Chlorophyll-a pigments with peak around 665 nm varied from 0.065 to 0.101 m^{-1} for Lake Markiezaatsmeer. With Lake Binnenschelde and Hulsbeek, the absorption coefficients of Chlorophyll-a pigments with peak around 440 nm varied from 0.132 to 0.297 m^{-1} and 0.323 to 0.559 m^{-1} while near 665 nm 0.080 to 0.168 m^{-1} and 0.153 to 0.264 m^{-1}respectively (see figure 5-2 for details).

a. How can we adapt a model such that it can use Landsat-8 OLI and SPOT6 MSI to estimate Chlorophyll-a concentration (absorption coefficients of Chlorophyll-a pigments/phytoplankton) and produce validated Chl-a images?

Based on the reflectance and absorption spectra characteristics of the study area, this study is able to adapt a model that can use Landsat-8 OLI and SPOT6 MSI to estimate Chlorophyll-a concentration (absorption coefficients of Chlorophyll-a pigments/phytoplankton). Four models were used and tested to estimate chlorophyll-a concentrations from both in-situ and satellite data (Landsat-8 and SPOT 6). These models had a direct relationship with Chl-a concentration. In the adaptation of the models both in-situ derived Rrs derived Rrs was applied directly with the models, however with Landsat-8 and SPOT 6, band simulation was performed to select the optimal bands for the application on the models since it does have some of the specified bands and wavelength required for the estimation of Chlorophyll-a. The actual bands used in this

study for the estimation of Chl-a using the specified models (MCI, 3B, NDCI and 4B) are presented in Appendix c. Hence based on band ratio-ing from this research using the band Rrs of Band 3, 4 and 5 for Landsat-8 and Bands 1, 2 and 3 for SPOT6, the MCI and 3B models had a good correlation with absorption of Chl-a pigments. They had an R^2 of 0.74 and 0.64 for Landsat-8 and 0.57 for MCI with SPOT6 Rrs concurrently.

b. Which model (based on performance) is best for the quantification and estimation of Chl-a in inland waters for the area under study?

The accuracy, performance and robustness of each of the four models were tested by validating the calibrated models, which was performed using TRIOS-RAMSES, Landsat-8 and SPOT6 reflectance (Rrs). The best fitting coefficients obtained from the calibrated equations was used to estimate/derive back the Chl-a absorption coefficient. This derived/estimated Chl-a absorption coefficients were regressed again against the measured in-situ chlorophyll-a absorption to see how they vary and to evaluate the performance and accuracy of each of the models using R^2 and rMAE.

From the adaptation of models, it was found that all the models worked well with both in-situ and Landsat-8 data (Rrs) but did not worked too well with SPOT6 data (Rrs). The model results proved that the only the MCI model, compared to other models (3B, NDCI, and 4B), is more robust and efficient in estimating Chl-a from inland lakes according this study. The MCI showed that it is very sensitive and accountable for any small variation between measured absorption Chl-a pigments and derived/estimated absorption Chl-a pigments. Although when the models were applied with in-situ data (Rrs), the four band model (4B/FBS) showed a stronger linear relationship with absorption Chl-a pigments with an R^2 of 0.83, and relative root mean error of 12.35% respectively. It was also found that, the models (3B, NDCI and 4B) failed to validate when applied SPOT data; they had a poor performance against measured absorption of Chl-a pigments. Both their calibrated and validated results were not displayed of analysis. Mostly, according to this study, models or algorithms that uses at least three bands or more gives a higher accuracy in estimating for Chl-a than less than three bands.

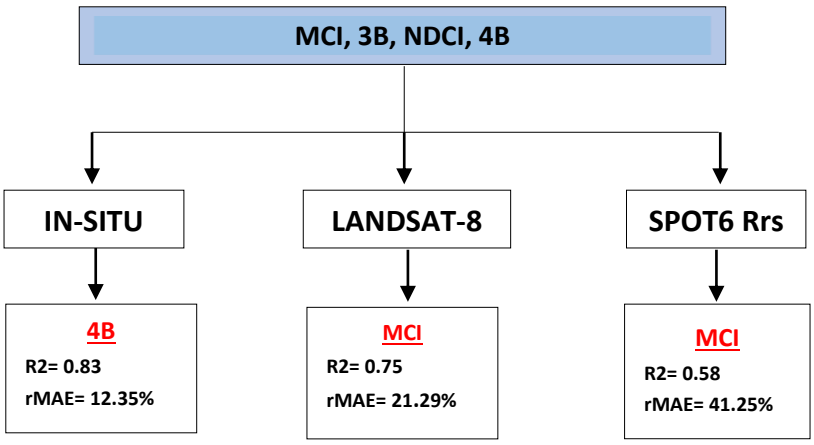

Figure 6-1: Model accuracy and performance based on application on different datasets.

Conceptualizing from the figure 6-1 above, it can be noted that with the application of the models on the various data sets (In-situ, Landsat-8 and SPOT6), the MCI model obtained a satisfactory results and came out to be the best when it was tuned using both satellite data. Although the 4B model was best model when applied to in-situ data with R^2, of 0.83, , MCI still proves to have a also a good correlation with R^2 and rMAE of 0.69 18.34 % with only 6 % increase in percentage between measured and derived/estimated absorption of Chl-a pigments.

c. How much error do In-situ, Landsat-8 and SPOT6 Multi-Spectral setup introduces in the derivation of Chl-a?

Before the launch of Landsat-8, many studies have utilized Landsat imagery for mapping water quality. However, the analysis of the spectro-radiometric sensitivity of landsat-8 OLI using the signal-to-noise ratio (SNR) as a guide gives a clue on the errors anticipated for the retrieval of biogeochemical properties such as Chl-a (Pahlevan et al., 2014). Signal-to-noise ratio (SNR) is a function of band location, band width and pixel size as well as the sensitivity of a sensor.

Regardless of the broad spectral bands of Landsat-8, this study demonstrated that Landsat-8 OLI bands (in this case Red, Green and NIR) are sensitive to the estimation and derivation of water constituents such as Chl-a and the error that it introduced was less as compared to the spectral bands of SPOT6. For example, when comparing the MCI model application on both the derived Rrs of In-situ data and convolved data, the validation results showed that the error percentage that Landsat-8 introduced to spectral setup in deriving Chl-a was almost 3% (with rMAE of 21.29%) when compared to In-situ setup (with rMAE of 18.34%). On the other hand, SPOT6 setup showed a much higher error in the derivation of absorption of Chl-a pigments with almost doubled percentage error of (with rMAE of 41.25%) than what Landsat-8 introduced to the derivation of Chl-a. The poor performance of the 3B, NDCI and 4B models from SPOT6 data for which results were not displayed may be due to a number of reasons; (a) the increment in error percentage between Landsat-8 and SPOT6 may be due to differences in SNR ratios of Landsat-8 and SPOT6; and (b) it can also be the inability of SPOT6 bands to optimally respond to absorption of Chl-a pigments.

Concurrently, figure 5-8 indicate that most of the models applied on Landsat-8 data seem to over-estimate absorption coefficient of chlorophyll-a pigments in all the lakes and this accounted for the high percentage in error for all the models compared to the error that in-situ setup introduced in the derivation of absorption coefficient of chlorophyll-a pigments. MCI and 3B, had an rMAE of 21.29%, 24.21%, as well as 32.68% for NDCI and 52.64% for the 4B model which introduced the highest percentage error in the derivation of absorption coefficient of chlorophyll-a pigments. However, the accuracy of the calibration and validation model results of SPOT6 spectral setup in deriving absorption coefficient of chlorophyll-a pigments was comprised with errors affected by the degradation of absorption coefficient of chlorophyll-a pigments, which was introduced especially by the type of atmospheric correction used.

However, on the basis of satellite comparison, Landsat-8 proved to be more accurate and sensitive to changes to the derivation of Chl-a and has the potential for studying bio-optical properties in coastal and inland waters (Pahlevan et al., 2014). This may be due to a number of factors including the enhancement of the Landsat-8 bands from 12 bits to 16 bits.

d. What is the gained knowledge of having a high resolution maps from Landsat-8 and SPOT6.

(Mapping of Chlorophyll-a (a_pig) from Landsat-8-OLI and SPOT6 MSI).

Based on the best adjudged model, for quantifying Chl-a maps were created using values from B3, B4, and B5 for Landsat-8 and B1, B2 and B3 for SPOT6 in Envi and ArcGIS software. The application of the best performing model to landsat-8-OLI is shown below in figures 6-2 and 6-3. Although six images were downloaded for this study on Binnenschelde and Markiezaatsmeer, only four of these images were cloud free taken on 4th April, 7th June, 3rd August, and 27th September, 2015. These maps shows an overview of the general Chl-a distribution in the lakes under study and can be used as a supportive information in the identifying eutrophication affected areas. They show a variability in the ecological and trophic status of the lakes under study with some degree of knowledge and accuracy in relation to the floating of algae bloom. Baban, (1999), indicated that changes in absorption of Chl-a pigments may be due to the amount of water leaving reflectance in the photosynthetically active region of the electromagnetic spectrum. However, this can only be detected using optical remote sensors (Baban, 1999). Absorption of Chl-a pigments colour maps in Lake Binnenschelde, Markiezaatsmeer and Hulsbeek varies from red (high a_chl-a) to blue (low a_chl-a) Figure 5-9 and 5-10 shows time series of absorption coefficients of Chl-a pigments maps calculated using MCI. According to the visualised MCI maps shown in figure 6-2 and 6-3, absorption coefficients of Chl-a pigments were uniformly distributed over the individual lakes. For Lake Binnenschelde, relatively higher Chl-a concentration were recorded in April and August while September recorded a moderate Chl-a concentration. This may be due to higher temperatures and lack of precipitation between April and August and vice versa for September.

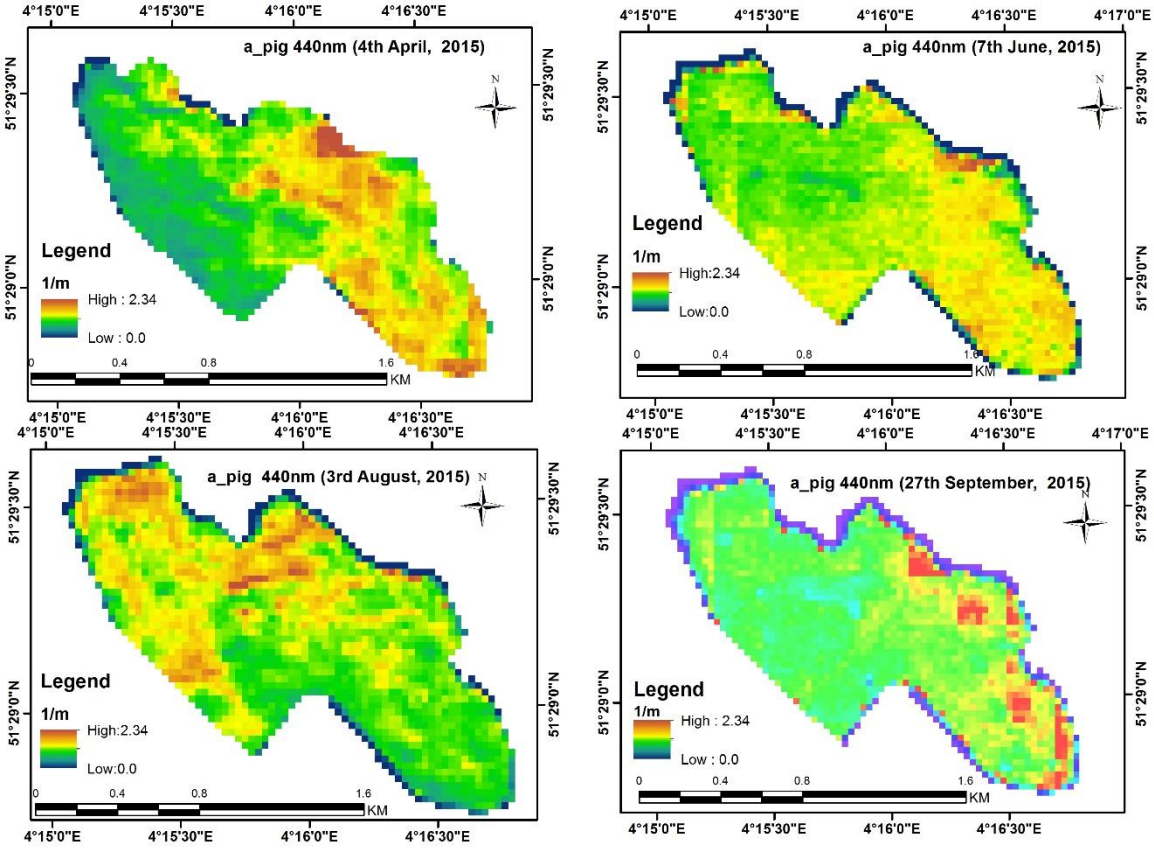

Figure 6-2: Absorption coefficients of Chlorophyll-a pigment maps created from Landsat-8 over Lake Binnenschelde on 4th April, 7th June, 3rd August, and 27th September, 2015.

The absorption coefficients of chlorophyll-a pigment maps that were created by the MCI model in figure 6-2 showed that the distribution and variation of absorption of chlorophyll-a pigments increases in the south-eastern part of Lake Binnenschelde on 4th April, 7th June and 27th September, 2015 and changes its variation in the map of 3rd August, 2015 from the south eastern part of the map to the north-western part of this same lake concurrently. Also in figure 6-3, it can be seen that most of the distribution and variations flows from north-western to south-eastern part of the Lake Markiezaatsmeer. All this may also be due to sunlight penetration which lead to increase in temperature and causes floating algae to keep changing places due to changes in wind direction as well as lack of precipitation respectively.

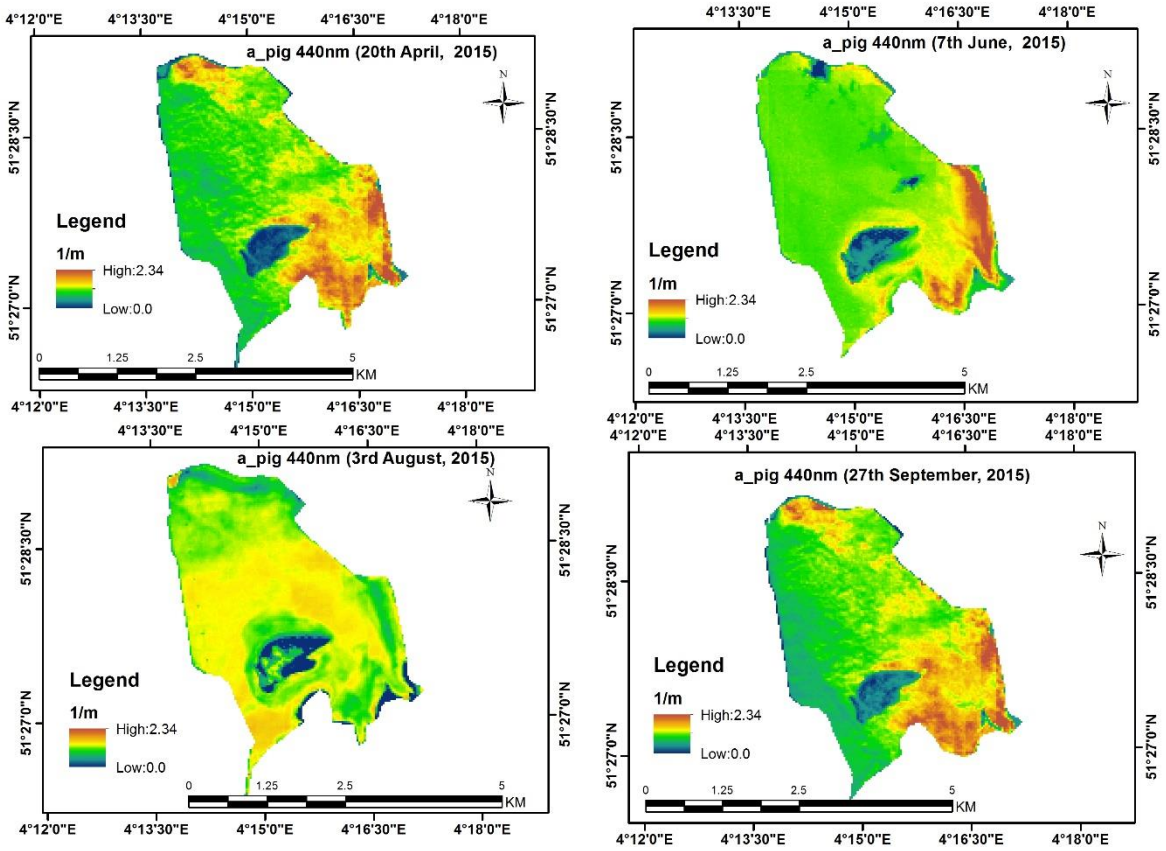

Figure 6-3: Absorption of Chlorophyll-a pigment maps created from Landsat-8 over Lake Markiezaatsmeer on 20th April, 7th June, 3rd August, and 27th September, 2015.

Moreover, the same approach was performed on atmospherically corrected SPOT6 images by applying MCI model. The variations in chlorophyll-a distribution depict differences in the sensor type. On the other hand, two SOPT6 images were downloaded for Binnenschelde and Markiezaatsmeer and one for Lake Hulsbeek, which were all cloud free taken on 2nd November and 4th December, 2015. They show a variability in the ecological and trophic status of the lakes under study with some degree of knowledge and accuracy in relation to the floating of algae bloom. The maps above indicates the distribution of absorption coefficients of Chl-a pigments for various days using MCI reflectance bands 3, 4 and 5 for Landsat-8 and bands 1, 2 and 3 for SPOT6. The SPOT6 images in figure 5-11 were also retrieved on 2nd November and 4th December respectively. Unfortunately only one SPOT6 image (figure 5-12) of Hulsbeek was processed and used to map Chl-a concentration. Landsat-8 image of Hulsbeek were not clear enough to be used to map Chl-a concentration (absorption of Chl-a) using MCI. The map of 20th April, 7th June and 27th September, 2015 shows high concentration of Chl-a (a_pig) in the south eastern part of Lake Markiezaatsmeer attributed to more sunlight penetration as discussed in figure 6-2.

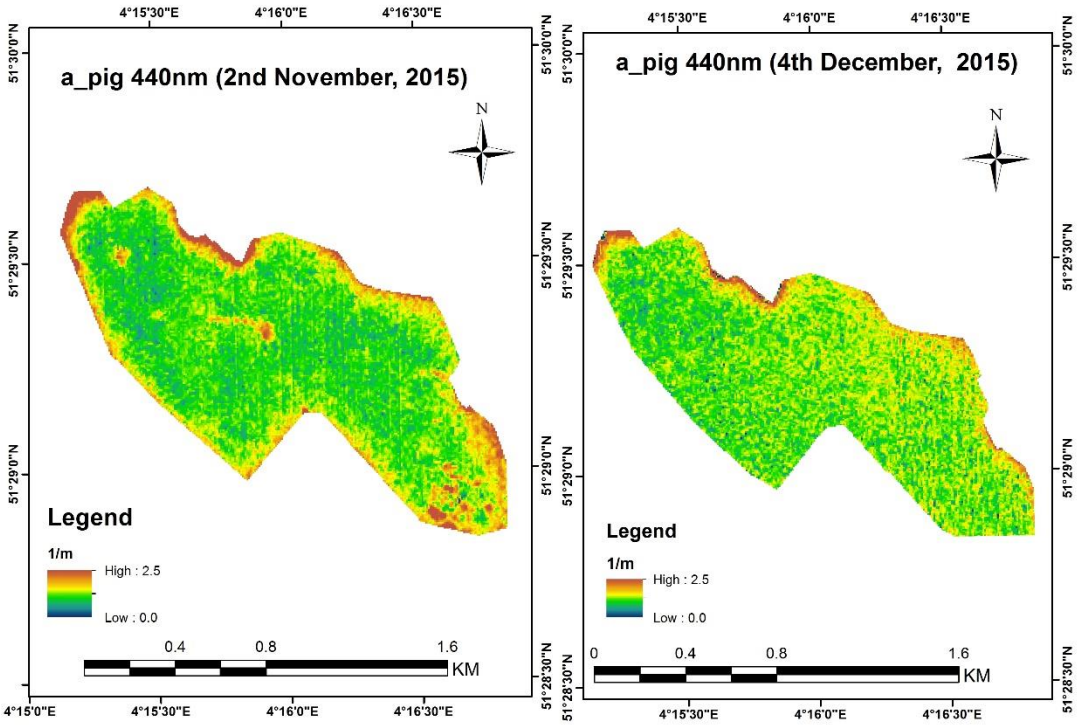

Figure 6-4: Absorption of Chlorophyll-a pigment maps created from SPOT6 over Lake Binnenschelde on 2nd November, and 4th December, 2015.

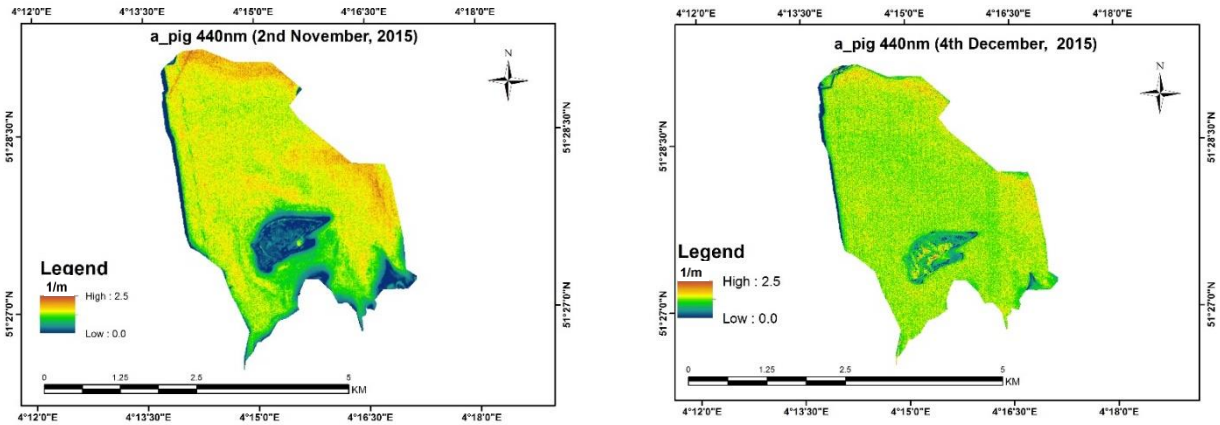

Figure 6-5: Absorption of Chlorophyll-a pigment maps created from SPOT6 over Lake Markiezaatsmeer on 2nd November, and 4th December, 2015.

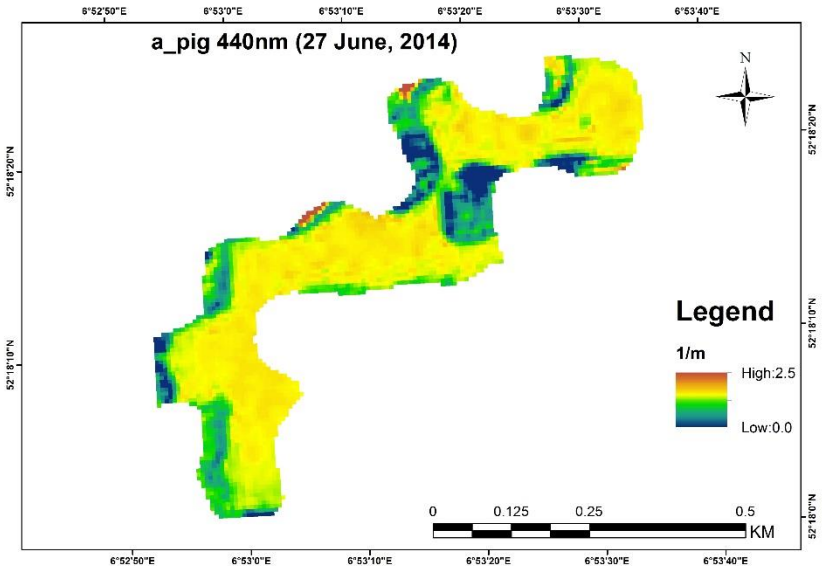

Figure 6-6: Absorption of Chlorophyll-a pigment maps created from SPOT6 over Lake Hulsbeek and on 2nd November, and 4th December, 2015.

These maps indicates fair distribution of chlorophyll-a absorption also computed from the MCI model using reflectance in the Band 1, 2 and 3. The red colour indicates high values of Chl-a absorption while the lowest values of Chl-a absorption on the map are shown in blue. The image of 2nd November shows more of value of Chl-a distribution in Lake Markiezaatsmeer and Binnenschelde also of the same date. On the other hand images of 4th December depict moderate (mostly in green) distribution of Chl-a absorption. The maps shows some eutrophication trends during spring (2nd November, 2015) while seem to be relatively normal during winter (4th December, 2015). Figure 5-12 shows high Chl-a absorption values over Lake Hulsbeek. Hence, Chl-a pigments absorption maps produced indicates that the MCI model can be used to monitor the distribution and variation of phytoplankton or chlorophyll-a pigments.

7. CONCLUSION AND RECOMMENDATIONS

7.2. CONCLUSION

Remote sensing provides an effective means to traditional water sampling for monitoring changes in water systems. Remote sensing is capable to provide accurate water quality information for an area.

However, from the above mentioned results, the following conclusions were made which form a basis in answering my research questions.

Different band combination gave different results in the estimation of Chl-a in inland lakes over the derived TRIOS in-situ reflectance and derived multispectral satellite image reflectance (Baig et al., 2013; Watanabe et al., 2015). The models were evaluated using data from TRIOS-RAMSES radiometric data with in-situ Chl-a absorption, Landsat-8 and SPOT6 convolved data. Mostly using more than three (3) bands combination seem to give a higher accuracy than using only two band combinations. For instance, the four band model and the MCI proves to be better than all other band combination in the NIR-Red wavelength spectrum (Baig et al., 2013). NDCI and 3B were not sensitive enough to estimate Chl-*a*.

On the other hand, when model/algorithm was applied on the various Landsat-8 and SPOT 6 data sets, results from Landsat-8 prove to be accurate for accurate estimation of Chl-*a* than the result from SPOT-6. The application of the model particularly on Landsat-8 data set showed quiet good results. It was indicated in tables 5-8 and 5-9 that when comparing the assessment evaluation for model application on Landsat -8 and SPOT 6, Maximum Chlorophyll Index model performed best in estimating Chl-a, although it could not produce same results when applied to the in-situ data. In all it was concluded that MCI model which worked with both Landsat-8 and SPOT6 when tested against in-situ derived chlorophyll-a and therefore was adjudged to be the best fitting model for estimating chlorophyll-a. In all, the 4B model performed well using TRIOS-RAMSES radiometric data with an R^2 of 0.83 and the lowest rMAE 12.35% compared R^2 of 0.75, and rMAE of 21.29% from the best chosen model MCI. However, the MCI model was chosen because of it compatibility in working across all data sets used in this study.

The MCI algorithms, is not to be undermined in such that it is seen to be a "versatile tool" and can be used in connection with other satellites to estimate Chl-a and other image analysis (Binding et al., 2013).

Secondly, FLAASH scheme seem to be more suitable for atmospheric correction of Landsat-8 images more than SPOT6 images hence the accuracy was very low for SPOT6 images. Band selection after atmospheric correction were also tested and based on that band shifting or tuning was executed to see which of the bands is sensitive to the estimation of Chl-a using the model application. On our finding, it was revealed that since

there is no bands of 709 and 753 in the Landsat 8 product, we shifted the selection of 708,709, and 753 to the NIR in band 5. The results of shifting bands gave a higher accuracy and hence it can be stated clearly that since there is no band for 700 nm – 790 nm band shifting could be possibly used to estimate Chl-a based on the findings of this studies. Accordingly, it can also be stated that a special atmospheric correction schemes should be used for a study of this sort. However, it can noted that the selected wavelengths for the model application differed slightly from previous studies as suggested by the original authors of the algorithms used in estimating Chl-a (Dall'Olmo & Gitelson, 2006). This could be that the reflectance spectra of the study areas differs from the spectra characteristics of the proposed algorithm from literature by the aforementioned authors.

Although band combination algorithms seem to be effective in estimation chlorophyll-a concentration using Landsat-8/SPOT6 product, it is still a challenge due to its limited spectral resolution.

The distribution maps of Chl-a absorption (Chl-a concentration) acquired by the best model (MCI) could be useful in analysing the Chl-a source as well as transport processes. However, the results of those study are limited to the study areas under study.

The study aimed at adapting and testing the performance of algorithms/models using Landsat-8-OLI and SPOT6 MSI with in-situ Chl-a absorption as well as determining the error each setup (in-situ, Landsat-8 and SPOT6) introduces to the derivation of Chl-a. It was found that MCI showed almost similar pattern for the various datasets and also had a better results with the lowest rMAE of 18.34%, 21.29% and 41.258% respectively. In short, the model analysis has demonstrated the first five bands of Landsat-8 sensor, especially bands 3, 4 and 5 can be used to estimate absorption coefficient of chlorophyll-a pigments in small lakes with relatively high accuracy. Again, better spectral resolution can be used since the wavelength bands used to estimate absorption coefficient of chlorophyll-a pigments in this study yielded satisfactory results for Landsat-8, they are not optimal for the detection of absorption coefficient of chlorophyll-a pigments in other settings (case II waters). In all, it can be stated that the remote sensing method used in this study could be used to map the spatial pattern and distribution of Chl-a in lakes Binnenschelde, Markiezaatsmeer and Hulsbeek using Landsat-8 and SPOT6 data and we anticipate to test this experiments in other lakes in the near future.

7.3. RECOMMENDATIONS

Basically, using other approaches other than application of empirical models can be investigated better for the estimation of Chl-a especially on SPOT6 datasets. Since the error related to SPOT6 sensor could not be improved in this study, focus should be on the testing and improvement of the various atmospheric correction methods for SPOT-6.

Finally, it should be noted that, none of the models used in this study was perfect and each of them had its own strengths and weaknesses. Hence, more studies must be completed to improve models in the selected study sites for this research for accurate estimates of absorption coefficient of chlorophyll-a pigments.

LIST OF REFERENCES

Alikas, K., Kangro, K., & Reinart, A. (2010). Detecting cyanobacterial blooms in large North European lakes using the maximum chlorophyll index. *Oceanologia*, *52*(2), 237–257. doi:10.5697/oc.52-2.237

Augusto-Silva, P. B., Ogashawara, I., Barbosa, C. C. F., de Carvalho, L. A. S., Jorge, D. S. F., Fornari, C. I., & Stech, J. L. (2014). Analysis of MERIS reflectance algorithms for estimating chlorophyll-a concentration in a Brazilian reservoir. *Remote Sensing*, *6*(12), 11689–11707. doi:10.3390/rs61211689

Baban, S. M. J. (1999). Use of remote sensing and geographical information systems in developing lake management strategies. *Hydrobiologia*, *396*(1), 211–226. Retrieved from https://www.researchgate.net/profile/Professor_Serwan_Baban/publication/227125681_Baban_S._M._J._Use_of_remote_sensing_and_geographical_information_systems_in_developing_lake_management_strategies._Hydrobiologia_395396/links/55955d5008ae793d137b1328.pdf

Barsi, J. A., Lee, K., Kvaran, G., Markham, B. L., & Pedelty, J. A. (2014). The spectral response of the Landsat-8 operational land imager. *Remote Sensing*, *6*(10), 10232–10251. doi:10.3390/rs61010232

Berni, J. A. J., Zarco-Tejada, P. J., Suárez, L., González-Dugo, V., & Fereres, E. (2009). Remote sensing of vegetation from UAV platforms using lightweight multispectral and thermal imaging sensors. *Int. Arch. Photogramm. Remote Sens. Spatial Inform. Sci*, *38*(6), 6 pp. doi:10.1007/s11032-006-9022-5

Binding, C. E., Greenberg, T. A., & Bukata, R. P. (2013). The MERIS Maximum Chlorophyll Index; its merits and limitations for inland water algal bloom monitoring. *Journal of Great Lakes Research*, *39*(S1), 100–107. doi:10.1016/j.jglr.2013.04.005

Blondeau-Patissier, D., Schroeder, T., Brando, V. E., Maier, S. W., Dekker, A. G., & Phinn, S. (2014). ESA-MERIS 10-year mission reveals contrasting phytoplankton bloom dynamics in two tropical regions of Northern Australia. *Remote Sensing*, *6*(4), 2963–2988. doi:10.3390/rs6042963

Bonansea, M., Ledesma, C., Rodríguez, C., Pinotti, L., & Antunes, M. H. (2015). Effects of atmospheric correction of Landsat imagery on lake water clarity assessment. *Advances in Space Research*, *56*(11), 2345–2355. doi:10.1016/j.asr.2015.09.018

Bricaud, A., Babin, M., Morel, A., & Claustre, H. (1995). Variability in the chlorophyll-specific absorption coefficients of natural phytoplankton: Analysis and parameterization. *Journal of Geophysical Research*, *100*(C7), 13321. doi:10.1029/95JC00463

Bricaud, A., Morel, A. Y., & Prieur, L. (1981). Absorption by dissolved organic matter of the sea (yellow substance) in the UV and visible domains. *Limnology and Oceanography*. doi:10.4319/lo.1981.26.1.0043

Cleveland, J. S., & Weidemann, a. D. (1993). Quantifying absorption by aquatic particles: A multiple scattering correction for glass-fiber filters. *Limnology and Oceanography*, *38*(6), 1321–1327. doi:10.4319/lo.1993.38.6.1321

Collin, A., & Hench, J. L. (2012). Towards Deeper Measurements of Tropical Reefscape Structure Using the WorldView-2 Spaceborne Sensor. *Remote Sensing*, *4*(5), 1425–1447. doi:10.3390/rs4051425

Cui, T., Zhang, J., Groom, S., Sun, L., Smyth, T., & Sathyendranath, S. (2010). Validation of MERIS ocean-color products in the Bohai Sea: A case study for turbid coastal waters. *Remote Sensing of Environment*, *114*(10), 2326–2336. doi:10.1016/j.rse.2010.05.009

D'Sa, E. J., Miller, R. L., & Del Castillo, C. (2006). Bio-optical properties and ocean color algorithms for coastal waters influenced by the Mississippi River during a cold front. *Applied Optics*, *45*(March), 7410–7428. doi:10.1364/AO.45.007410

Dall'Olmo, G., & Gitelson, A. A. (2006). Effect of bio-optical parameter variability and uncertainties in reflectance measurements on the remote estimation of chlorophyll-a concentration in turbid productive waters: modeling results. *Applied Optics*, *45*(15), 3577–3592. doi:10.1364/AO.45.003577

Dall'Olmo, G., Gitelson, A. A., Rundquist, D. C., Leavitt, B., Barrow, T., & Holz, J. C. (2005). Assessing the potential of SeaWiFS and MODIS for estimating chlorophyll concentration in turbid productive waters using red and near-infrared bands. *Remote Sensing of Environment*, *96*(2), 176–187. doi:10.1016/j.rse.2005.02.007

Dall'Olmo, Giorgio. Gitelson, A, A. Rundquist, Donald, C. (2003). Towards a unified approach for remote estimation of chlorophyll-a in both terrestrial vegetation and turbid productive waters. *Geophysical Research Letters*, *30*(18), 8–11. doi:10.1029/2003GL018065

Darecki, M., Kaczmarek, S., & Olszewski, J. (2005). SeaWiFS ocean colour chlorophyll algorithms for the southern Baltic Sea. *International Journal of Remote Sensing*, *26*(June 2014), 247–260. doi:10.1080/01431160410001720298

El-Alem, A., Chokmani, K., Laurion, I., & El-Adlouni, S. E. (2012). Comparative analysis of four models to estimate chlorophyll-a concentration in case-2 waters using MODerate resolution imaging spectroradiometer (MODIS) imagery. *Remote Sensing*, *4*(8), 2373–2400. doi:10.3390/rs4082373

Feng, L., Hu, C., Han, X., Chen, X., & Qi, L. (2014). Long-Term Distribution Patterns of Chlorophyll-a Concentration in China's Largest Freshwater Lake: MERIS Full-Resolution Observations with a Practical Approach. *Remote Sensing*, *7*(1), 275–299. doi:10.3390/rs70100275

Gitelson, A. A, Gurlin, D., Moses, W. J., & Barrow, T. (2009). A bio-optical algorithm for the remote estimation of the chlorophyll- a concentration in case 2 waters. *Environmental Research Letters*, *4*(4), 045003. doi:10.1088/1748-9326/4/4/045003

Gitelson, A. A., Dall'Olmo, G., Moses, W., Rundquist, D. C., Barrow, T., Fisher, T. R., … Holz, J. (2008). A simple semi-analytical model for remote estimation of chlorophyll-a in turbid waters: Validation. *Remote Sensing of Environment*, *112*(9), 3582–3593. doi:10.1016/j.rse.2008.04.015

Gitelson, A. A., Schalles, J. F., & Hladik, C. M. (2007). Remote chlorophyll-a retrieval in turbid, productive estuaries: Chesapeake Bay case study. *Remote Sensing of Environment*, *109*(4), 464–472. doi:10.1016/j.rse.2007.01.016

Gitelson, A. A., Yacobi, Y. Z., Schalles, J. F., Rundquist, D. C., Han, L., Stark, R., & Etzion, D. (2000). Remote estimation of phytoplankton density in productive waters. *Limnology and Lake Management - Archives for Hydrobiolia, Special Issues, Advances in Limnology*. Retrieved from http://www.calmit.unl.edu/people/agitelson2/pdf/14_Arch_Hydrobiol-2000.pdf

Gordon, H. R., Clark, D. K., Brown, J. W., Brown, O. B., Evans, R. H., & Broenkow, W. W. (1983). Phytoplankton pigment concentrations in the Middle Atlantic Bight: comparison of ship determinations and CZCS estimates. *Applied Optics*, *22*(1), 20–36. doi:10.1364/AO.22.000020

Gower, J., King, S., Borstad, G., & Brown, L. (2005). Use of the 709 nm band of meris to detect intense plankton blooms and other conditions in coastal waters. *European Space Agency, (Special Publication) ESA SP*, (572), 365–368. doi:10.1080/01431160500075857

Gower, J., King, S., & Goncalves, P. (2008). Global monitoring of plankton blooms using MERIS MCI. *International Journal of Remote Sensing*, *29*(21), 6209–6216. doi:10.1080/01431160802178110

Groetsch, P. M. M., Simis, S. G. H., Eleveld, M. A., & Peters, S. W. M. (2014). Cyanobacterial bloom detection based on coherence between ferrybox observations. *Journal of Marine Systems*, *140*, 50–58. doi:10.1016/j.jmarsys.2014.05.015

Guanter, L., Ruiz-Verdú, A., Odermatt, D., Giardino, C., Simis, S., Estellés, V., … Moreno, J. (2010). Atmospheric correction of ENVISAT/MERIS data over inland waters: Validation for European lakes. *Remote Sensing of Environment*, *114*(3), 467–480. doi:10.1016/j.rse.2009.10.004

Gurlin, D., Gitelson, A. A., & Moses, W. J. (2011). Remote estimation of chl-a concentration in turbid productive waters - Return to a simple two-band NIR-red model? *Remote Sensing of Environment*, *115*(12), 3479–3490. doi:10.1016/j.rse.2011.08.011

Heisler, J., Glibert, P. M., Burkholder, J. M., Anderson, D. M., Cochlan, W., Dennison, W. C., … Suddleson, M. (2008). Eutrophication and harmful algal blooms: A scientific consensus. *Harmful Algae*, *8*(1), 3–13. doi:10.1016/j.hal.2008.08.006

Huang, C. C., Li, Y. M., Yang, H., Wang, Q., Li, J. S., & Chen, X. (2013). Underwater light field determined by water constituents in highly turbid water: The case of Taihu lake. *Journal of Limnology*, *72*(1), 21–34. doi:10.4081/jlimnol.2013.e3

Huang, Y., Jiang, D., Zhuang, D., & Fu, J. (2010). Evaluation of hyperspectral indices for chlorophyll-a concentration estimation in Tangxun lake (Wuhan, China). *International Journal of Environmental Research and Public Health*, *7*(6), 2437–2451. doi:10.3390/ijerph7062437

IOCCG. (2006). *IOCCG Report Number 05: Reports of the International Ocean-Colour Coordinating Group Remote Sensing of Inherent Optical Properties: Fundamentals, Tests of Algorithms, and Applications*. *IOCCG Report 5* (Vol. 5). doi:10.1006/jmbi.1998.2073

Kamerosky, A., Cho, H., & Morris, L. (2015). Monitoring of the 2011 Super Algal Bloom in Indian River Lagoon, FL, USA, Using MERIS. *Remote Sensing*, *7*(2), 1441–1460. doi:10.3390/rs70201441

Kudela, R. M. (2015). Harmful Algal Blooms A scientific summary for policy makers. *IOC/UNESCO*, (Paris (IOC/INF-1320). Retrieved from http://unesdoc.unesco.org/images/0023/002334/233419e.pdf

Kutser, T., Pierson, D. C., Kallio, K. Y., Reinart, A., & Sobek, S. (2005). Mapping lake CDOM by satellite remote sensing. *Remote Sensing of Environment*, *94*(4), 535–540. doi:10.1016/j.rse.2004.11.009

Lapointe, B. E., Herren, L. W., Debortoli, D. D., & Vogel, M. A. (2015). Evidence of sewage-driven eutrophication and harmful algal blooms in Florida's Indian River Lagoon. *Harmful Algae*, *43*, 82–102. doi:10.1016/j.hal.2015.01.004

Le, C., Li, Y., Zha, Y., Sun, D., Huang, C., & Lu, H. (2009). A four-band semi-analytical model for estimating chlorophyll a in highly turbid lakes: The case of Taihu Lake, China. *Remote Sensing of Environment*, *113*(6), 1175–1182. doi:10.1016/j.rse.2009.02.005

Ma, R., Tang, J., Dai, J., Zhang, Y., & Song, Q. (2006). Absorption and scattering properties of water body in Taihu Lake, China: absorption. *International Journal of Remote Sensing*, *27*(October 2014), 4277–4304. doi:10.1080/01431160600851835

Majozi, N. P., Salama, M. S., Bernard, S., Harper, D. M., & Habte, M. G. (2014). Remote sensing of euphotic depth in shallow tropical inland waters of Lake Naivasha using MERIS data. *Remote Sensing of Environment*, *148*, 178–189. doi:10.1016/j.rse.2014.03.025

Matsushita, B., Yang, W., Yu, G., Oyama, Y., Yoshimura, K., & Fukushima, T. (2015). A hybrid algorithm for estimating the chlorophyll-a concentration across different trophic states in Asian inland waters. *ISPRS Journal of Photogrammetry and Remote Sensing*, *102*, 28–37. doi:10.1016/j.isprsjprs.2014.12.022

Megard, R. O., Settles, J. C., Boyer, H. a, & Combs, W. S. (1980). Light, Secchi disks, and trophic states. *Limnology and Oceanography*, *25*(2), 373–377. doi:10.4319/lo.1980.25.2.0373

Mishra, S., & Mishra, D. R. (2012). Normalized difference chlorophyll index: A novel model for remote estimation of chlorophyll-a concentration in turbid productive waters. *Remote Sensing of Environment*, *117*, 394–406. doi:10.1016/j.rse.2011.10.016

Mitchell, B. G., Bricaud, A., Carder, K., Cleveland, J., & Ferrari, G. (2000). *Determination of spectral absorption coefficients of particles , dissolved material and phytoplankton for discrete water samples*. *Ocean Optics Protocols For Satellite Ocean Color Sensor Validation , Revision 2*. doi:NASA/TM–2000–209966

Mobley, C. D. (1999). Estimation of the remote-sensing reflectance from above-surface measurements. *Applied Optics*, *38*(36), 7442–7455. doi:10.1364/AO.38.007442

Mobley, C. D. (1999). Estimation of the remote-sensing reflectance from above-surface measurements. *Applied Optics*, *38*(36), 7442–7455. doi:10.1364/AO.38.007442

Montes-Hugo, M. a., Vernet, M., Martinson, D., Smith, R., & Iannuzzi, R. (2008). Variability on phytoplankton size structure in the western Antarctic Peninsula (1997–2006). *Deep Sea Research Part II: Topical Studies in Oceanography*, *55*(18-19), 2106–2117. doi:10.1016/j.dsr2.2008.04.036

Moreira, C., Ramos, V., Azevedo, J., & Vasconcelos, V. (2014). Methods to detect cyanobacteria and their toxins in the environment. *Applied Microbiology and Biotechnology*, *98*(19), 8073–8082. doi:10.1007/s00253-014-5951-9

Morel, A., & Prieur, L. (1977). Analysis of variations in ocean color. *Limnology and Oceanography*, *22*(4), 709–722. doi:10.4319/lo.1977.22.4.0709

O'Reilly, J. E., Maritorena, S., Mitchell, B. G., Siegel, D. A., Carder, K. L., Garver, S. A., … McClain, C. (1998). Ocean color chlorophyll algorithms for SeaWiFS. *Journal of Geophysical Research*, *103*(C11), 24937–24953. doi:10.1029/98JC02160

Pahlevan, N., Wei, J., Schaaf, C. B., & Schott, J. R. (2014). Evaluating radiometric sensitivity of Landsat 8 over coastal/inland waters. *International Geoscience and Remote Sensing Symposium (IGARSS)*, (IEEE International), 1393–1396. doi:10.1109/IGARSS.2014.6946695

Palmer, S. C. J., Kutser, T., & Hunter, P. D. (2015). Remote sensing of inland waters: Challenges, progress and future directions. *Remote Sensing of Environment*, *157*, 1–8. doi:10.1016/j.rse.2014.09.021

Rantajärvi, E., Olsonen, R., Hällfors, S., Leppänen, J.-M., & Raateoja, M. (1998). Effect of sampling frequency on detection of natural variability in phytoplankton: unattended high-frequency measurements on board ferries in the Baltic Sea. *Journal of Marine Science*, *55*(4), 697–704. doi:10.1006/jmsc.1998.0384

Rundquist, D. C., Han, L., Schalles, J. F., & Peake, J. S. (1996). Remote Measurement of Algal Chlorophyll in Surface Waters : The Case for the First Derivative of Reflectance Near 690 nm. *Photogrammetric Engineering & Remote Sensing*, *62*(2), 195–200.

Salama, M. S., Van Der Velde, R., Van Der Woerd, H. J., Kromkamp, J. C., Philippart, C. J. M., Joseph, A. T., … Su, Z. (2012). Technical Note: Calibration and validation of geophysical observation models. *Biogeosciences*, *9*(6), 2195–2201. doi:10.5194/bg-9-2195-2012

Song, K., Li, L., Wang, Z., Liu, D., Zhang, B., Xu, J., … Wang, Y. (2012). Retrieval of total suspended matter (TSM) and chlorophyll-a (Chl-a) concentration from remote-sensing data for drinking water resources. *Environmental Monitoring and Assessment*, *184*(3), 1449–1470. doi:10.1007/s10661-011-2053-3

Sun, D., Hu, C., Qiu, Z., & Shi, K. (2015). Estimating phycocyanin pigment concentration in productive inland waters using Landsat measurements: a case study in Lake Dianchi. *Optics Express*, *23*(3), 3055–3074. doi:10.1364/OE.23.003055

Survey, U. S. G. (2015). Landsat — Earth Observation Satellites Landsat Missions : Imaging the Earth Since 1972, (November), 2013–2016. Retrieved from http://pubs.usgs.gov/fs/2015/3081/fs20153081.pdf

Teneva, I., Mladenov, R., Belkinova, D., Dimitrova-Dyulgerova, I., & Dzhambazov, B. (2010). Phytoplankton community of the drinking water supply reservoir Borovitsa (South Bulgaria) with an emphasis on cyanotoxins and water quality. *Central European Journal of Biology*, *5*(2), 231–239. doi:10.2478/s11535-010-0009-1

Thiemann, S., & Kaufmann, H. (2000). Determination of chlorophyll content and trophic state of lakes using field spectrometer and IRS-1C satellite data in the Mecklenburg Lake District, Germany. *Remote Sensing of Environment*, *73*(2), 227–235. doi:10.1016/S0034-4257(00)00097-3

Tian, H., Cao, C., Xu, M., Zhu, Z., Liu, D., Wang, X., & Cui, S. (2014). Estimation of chlorophyll- *a* concentration in coastal waters with HJ-1A HSI data using a three-band bio-optical model and validation. *International Journal of Remote Sensing*, *35*(16), 5984–6003. doi:10.1080/01431161.2014.934403

Usgs/Doi. (2013). Landsat — A Global Land-Imaging Mission. *USGS Fact Sheet 2012*, (May). Retrieved from http://pubs.usgs.gov/fs/2012/3072/fs2012-3072.pdf

Van Dam, H. Mertens, A. (2013). Dutch lakes suffer from eutrophication | Airclim. Retrieved February 12, 2016, from http://airclim.org/acidnews/dutch-lakes-suffer-eutrophication

Vanhellemont, Q., & Ruddick, K. (2015). Advantages of high quality SWIR bands for ocean colour processing: Examples from Landsat-8. *Remote Sensing of Environment*, *161*, 89–106. doi:10.1016/j.rse.2015.02.007

Watanabe, F. S. Y., Alcântara, E., Rodrigues, T. W. P., Imai, N. N., Barbosa, C. C. F., & Rotta, L. H. D. S. (2015). Estimation of chlorophyll-a concentration and the trophic state of the barra bonita hydroelectric reservoir using OLI/landsat-8 images. *International Journal of Environmental Research and Public Health*, *12*(9), 10391–10417. doi:10.3390/ijerph120910391

Yang, X., Wu, X., Hao, H., & He, Z. (2008). Mechanisms and assessment of water eutrophication. *Journal of Zhejiang University. Science. B*, *9*(3), 197–209. doi:10.1631/jzus.B0710626

Yi, C. (2013). A Weighted Algorithm for Estimating Chlorophyll-a Concentration from Turbid Waters. *Journal of the Indian Society of Remote Sensing*, *41*(4), 957–967. doi:10.1007/s12524-013-0280-5

Yu, G., Yang, W., Matsushita, B., Li, R., Oyama, Y., & Fukushima, T. (2014). Remote Estimation of Chlorophyll-a in Inland Waters by a NIR-Red-Based Algorithm: Validation in Asian Lakes. *Remote Sensing*, *6*(1), 3492–3510. doi:10.3390/rs6043492

Zimba, P. V., & Gitelson, A. (2006). Remote estimation of chlorophyll concentration in hyper-eutrophic aquatic systems: Model tuning and accuracy optimization. *Aquaculture*, *256*(1-4), 272–286. doi:10.1016/j.aquaculture.2006.02.038

8. APPENDICES

Appendix A: Location and coordinates of Sample sites.

Dates	Sample points	Latitude (Decimal Degrees)	Longitude (Decimal Degrees)	Time Interval (GMT)
23-09-2015	**BN- S 1**	51°29'05.8"	4°16'34.5"	11:10
	BN-S 2	51°29'03.0"	4°16'39.2"	11:18
	BN-S 3	51°28'59.0"	4°16'41.7"	11:22
	BN-S 4	51°28'54.6"	4°16'43.5"	11:29
	BN-S 5	51°28'48.8"	4°16'44.0"	11:34
	BN-S 6	51°28'48.3"	4°16'33.1"	12:49
	BN-S 7	51°28'50.6"	4°16'28.4"	12:53
	BN-S 8	51°29'02.9"	4°16'11.8"	12:59
	BN-S 9	51°28'57.5"	4°15'48.8"	13:04
	BN-S 10	51°29'12.3"	4°15'34.4"	13:09
	BN-S 11	51°29'29.0"	4°15'25.3"	13:14
	BN-S 12	51°29'25.4"	4°15'28.1"	13:19
	BN-S 13	51°29'20.2"	4°16'11.1"	13:31
	BN-S 14	51°29'09.2"	4°16'33.9"	13:36
	BN-S 15	51°29'07.0"	4°16'28.9"	13:42

Dates	Sample points	Latitude (Decimal Degrees)	Longitude (Decimal Degrees)	Time Interval (GMT)
24-09-2015	**MK-S 16**	51°28'52.6"	4°13'50.3"	10:09
	MK -S 17	51°28'51.4"	4°14'13.5"	10:20
	MK -S 18	51°28'42.5"	4°14'45.7"	10:31
	MK -S 19	51°28'34.5"	4°15'17.0"	10:44
	MK -S 20	51°28'12.5"	4°16'15.7"	10:57
	MK -S 21	51°27'54.8"	4°16'35.0"	11:14
	MK -S 22	51°27'51.8"	4°16'22.9"	11:23
	MK -S 23	51°27'34.3"	4°16'35.5"	11:33
	MK -S 24	51°27'33.4"	4°16'37.4"	11:48

	MK -S 25	51°27'36.5"	4°16'23.7"	11:59
	MK -S 26	51°27'42.3"	4°16'06.3"	12:12
	MK -S 27	51°27'50.5"	4°15'52.8"	12:21
	MK -S 28	51°28'01.7"	4°15'42.1"	12:30
	MK -S 29	51°28'13.0"	4°15'38.8"	12:41
	MK -S 30	51°28'16.9"	4°15'24.6"	12:49
	MK -S 31	51°28'26.6"	4°15'16.3"	12:57
	MK -S 32	51°28'37.7"	4°15'14.3"	13:05
	MK -S 33	51°28'47.1"	4°15'05.8"	13:12
	MK -S 34	51°28'52.8"	4°14'46.5"	13:20
	MK -S 35	51°28'52.0"	4°14'18.8"	13:28

Dates	Sample points	Latitude (Decimal Degrees)	Longitude (Decimal Degrees)	Time Interval (GMT)
26-09-2015	**HL-S 36**	52°18'02.1''	6°52'58.9''	11:42
	HL-S 37	52°18'05.3''	6°52'59.2''	11:48
	HL-S 38	52°18'05.5''	6°52'58.9''	11:53
	HL-S 40	52°18'09.3''	6°52'53.3''	12:02
	HL-S 41	52°18'09.5''	6°52'56.8''	12:10
	HL-S 42	52°18'14.5''	6°53'00.2''	12:16
	HL-S 43	52°18'13.5''	6°53'05.8''	12:21
	HL-S 44	52°18'13.4''	6°53'17.2''	12:26
	HL-S 45	52°18'18.3''	6°53'16.1''	12:34
	HL-S 46	52°18'20.2''	6°53'23.9''	12:41
	HL-S 47	52°18'20.6''	6°53'30.2''	12:46

APPENDIX B: Figures showing how field measurements were conducted in Lake Binnenschelde, Lake Markiezaatsmeer and Lake Hulsbeek. Also shows the colour of the lakes (study area).

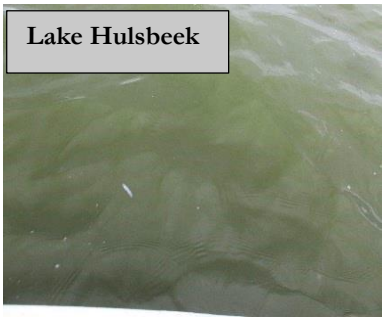

APPENDIX C: Calibration Results.

a. CALIBRATION RESULTS FROM IN-SITU DATA

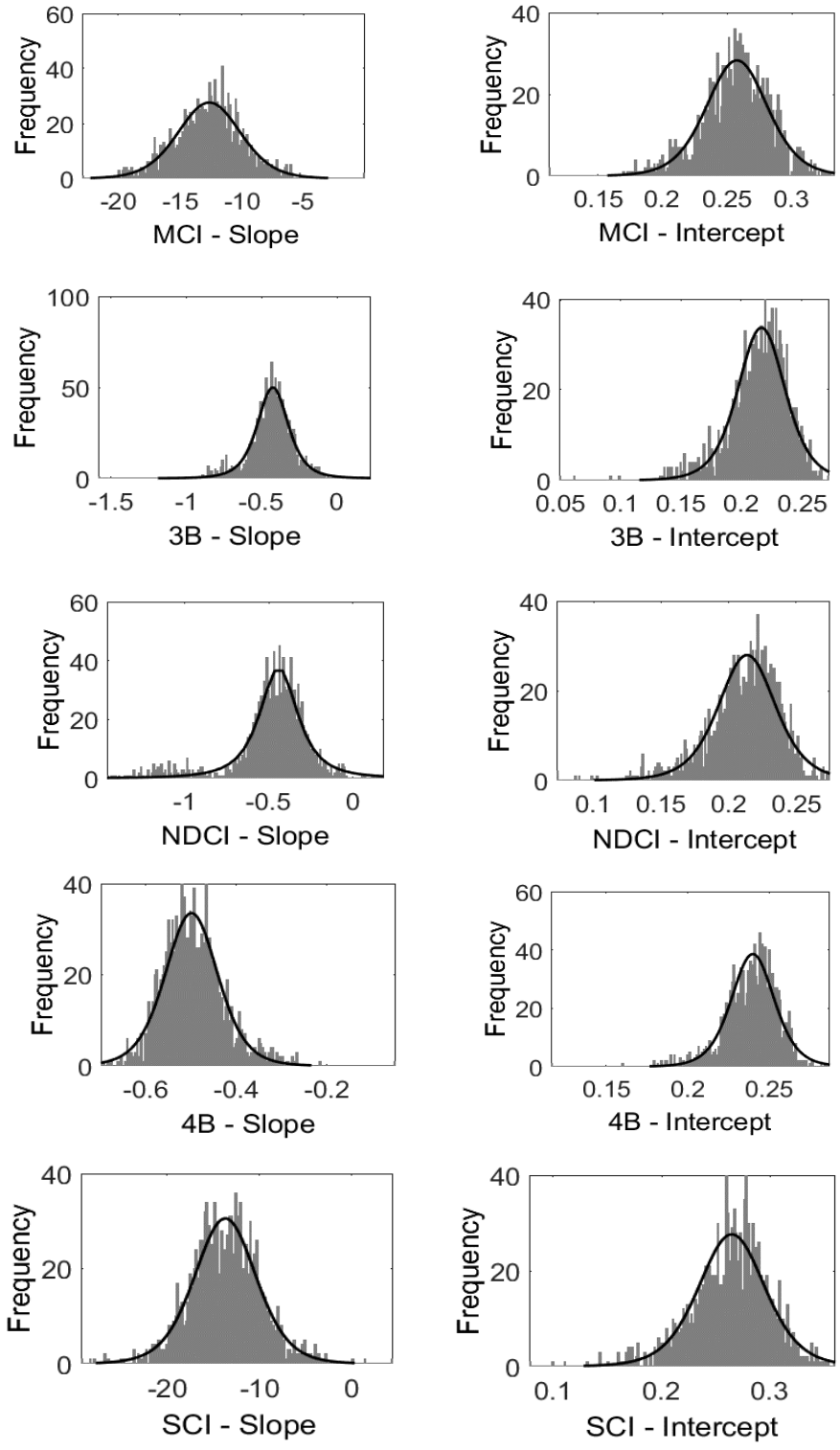

Figure 5-4 shows calibration process and their probability distribution of fitting coefficients for MCI, 3B, NDCI, 4B and SCI models or algorithms using field data.

b. CALIBRATION RESULTS FROM LANDSAT-8

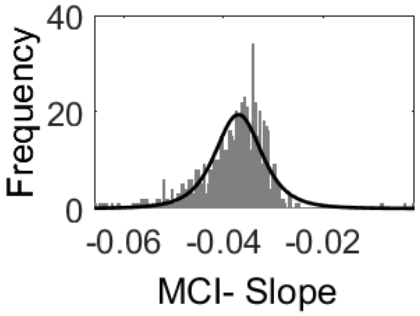

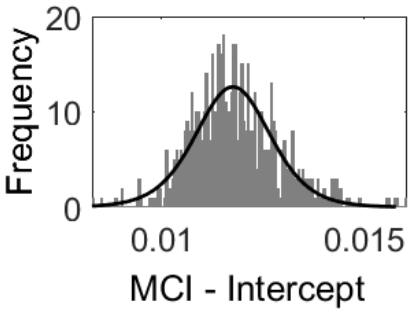

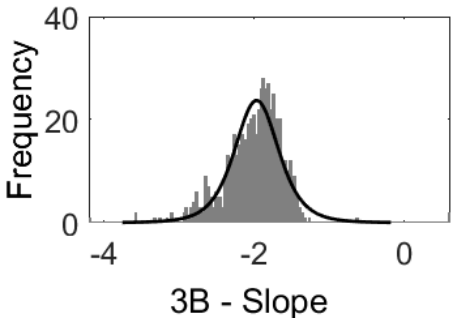

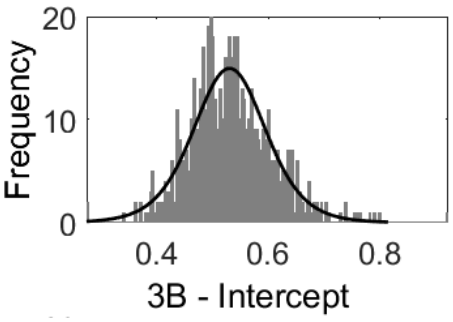

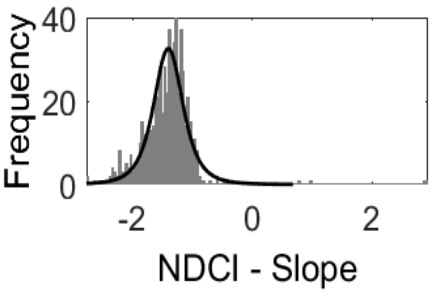

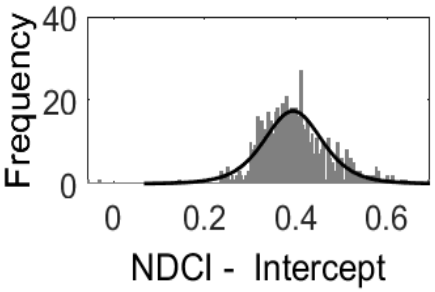

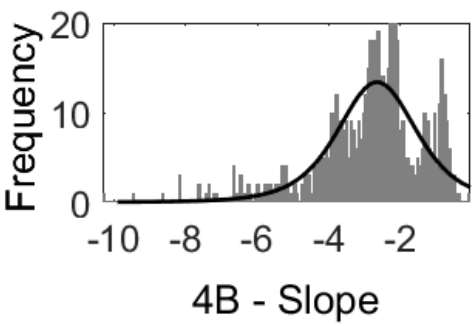

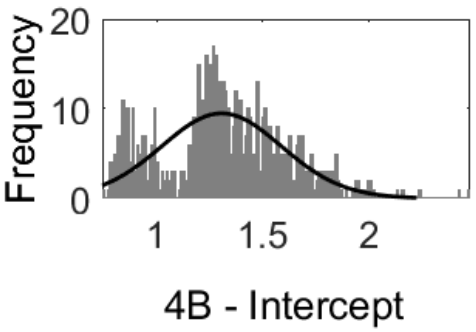

Appendix D. Band selection and combination from Satellite Data

a. Landsat-8-OLI.

Model Abbreviation	Bands Combination
MCI	$Rrs(B_4) - Rrs(B_3) * \left[\frac{(B_3 - B_4)}{(B_5 - B_4)}\right] * Rrs(B_5) - Rrs(B_4)$
N3B	$[Rrs^{-1}(B_3) - Rrs^{-1}(B_4)] * Rrs(B_5)$
NDCI	$\left[\frac{Rrs(B_5) - Rrs(B_4)}{Rrs(B_5) + Rrs(B_4)}\right]$
4B	$[Rrs^{-1}(B_4) - Rrs^{-1}(B_5)] * [Rrs^{-1}(B_4) - Rrs^{-1}(B_3)]^{-1}$

b. SPOT6.

Model Abbreviation	Bands Combination
MCI	$Rrs(B_2) - Rrs(B_1) * \left[\frac{(B_1 - B_2)}{(B_3 - B_2)}\right] * Rrs(B_3) - Rrs(B_2)$
N3B	$[Rrs^{-1}(B_1) - Rrs^{-1}(B_2)] * Rrs(B_3)$
NDCI	$\left[\frac{Rrs(B_3) - Rrs(B_2)}{Rrs(B_3) + Rrs(B_2)}\right]$
4B	$[Rrs^{-1}(B_2) - Rrs^{-1}(B_1)] * [Rrs^{-1}(B_3) - Rrs^{-1}(B_1)]^{-1}$